

Supplementary Information

A new class of anionic metallohelicates based on salicylic and terephthalic acid units, accessible in solution and by mechanochemistry

Jean-Louis Do,^{ab} Hatem M. Titi,^b Louis A. Cuccia,^{a} and Tomislav Friščić^{b*}*

a) Concordia University, Department of Chemistry and Biochemistry, 7141 Sherbrooke St. West, H4B 1R6, Montréal, Québec, Canada

b) McGill University, Department of Chemistry, 801 Sherbrooke St., H3A 0B8 Montréal, Québec, Canada

**Email: louis.cuccia@concordia.ca, tomislav.friscic@mcgill.ca*

Table of Contents

1. Experimental.....	3
1.1 Synthesis of <i>N,N'</i> -bis(3-carboxy-2-hydroxyphenyl)terephthalamide (H ₄ L)	3
1.2 Solution synthesis of Fe-H1	4
1.3 Solution synthesis of Fe-H2	4
1.4 Solution synthesis of Fe-H3	4
1.5 Solution synthesis of Fe-H4A	4
1.6 Solution synthesis of Fe-H4B.....	4
1.7 Solution synthesis of Fe-H4C.....	5
1.8 Solution synthesis of Cu-H1.....	5
1.9 Solution synthesis of Cu-H2.....	5
1.10 General procedure for the mechanochemical synthesis of helicates	5
1.11 Mechanochemical synthesis of Fe-H1	5
1.12 Mechanochemical synthesis of Fe-H2.....	6
1.13 Mechanochemical synthesis of Fe-H3.....	6
1.14 Mechanochemical synthesis of Fe-H4A	6
1.15 Mechanochemical synthesis of Fe-H4C	6
1.16 Mechanochemical synthesis of Cu-H1	6
1.17 Mechanochemical synthesis of Cu-H2	6
2. Summary of IR, ¹ H and ¹³ C NMR and HR-MS Data.....	7
3. ¹ H and ¹³ C-NMR Spectra.....	10
4. Fourier-Transform Attenuated Total Reflectance (FTIR-ATR) Spectra.....	12
5. Powder X-Ray Diffraction (PXRD) Patterns	20
6. HR-MS Spectra.....	26
7. Single Crystal X-ray Diffraction Data	40
8. Thermogravimetric analysis	49
9. References.....	52

1. Experimental

Unless otherwise specified, all reagents and solvents were purchased from commercial sources and used without further purification. Solution reactions were carried out in 6 dram borosilicate glass vials using a pre-programmed thermostat oven for any reaction temperatures above room temperature. Solid-state mechanochemical milling reactions were carried out in a Retsch MM200 mill operating at a frequency of 25 Hz using a 5 mL FTS stainless steel milling jar charged with a single stainless-steel ball bearing (7 mm diameter, 0.7 g). PXRD spectra were obtained in the 2θ range from 5° to 40° using a Bruker D2 PHASER X-Ray Diffractometer equipped with a $\text{CuK}\alpha$ ($\lambda = 1.54 \text{ \AA}$) source, LinxEye detector, and a Ni filter. FTIR-ATR spectra were obtained in the 400 cm^{-1} to 4000 cm^{-1} range on a Bruker VERTEX 70/70v FTIR spectrometer equipped with a Platinum ATR module. ^1H and ^{13}C NMR spectra were obtained on a Varian MERCURY plus-300 spectrometer (300 MHz) and a Bruker AVIIIHD 500 spectrometer (500 MHz), respectively, with chemical shifts (δ) given in parts per million (ppm). Confirmation of helicate formation was obtained using high-resolution mass spectrometry in negative mode on a Bruker MaXis API QqTOF with multiple charging ESI and direct probing capabilities in the 50-3000 m/z range. Thermogravimetric analysis and differential scanning calorimetry (TGA/DSC) data were measured on a TGA/DSC 1 (Mettler-Toledo, Columbus, Ohio, USA) instrument. All measurements were carried out under a 25 mL min^{-1} stream of air, and the samples were heated from RT up to 700°C using a constant heating ramp of $10^\circ\text{C min}^{-1}$.

1.1 Synthesis of *N,N'*-bis(3-carboxy-2-hydroxyphenyl)terephthalamide (H4L)

Tetrahydrofuran (THF) and dimethylformamide (DMF) were dried over molecular sieves for a minimum of 12 hours prior to use. In a 100 mL Erlenmeyer flask charged with a magnetic stir bar, 3-aminosalicylic acid (1.50 g, 9.79 mmol) was suspended in THF (50 mL) and placed under magnetic stirring. Solid terephthaloyl chloride (0.663 g, 3.26 mmol) was added to the mixture. Suspended solids rapidly dissolved, resulting in the formation of a dark brown solution and subsequent precipitation of a light pinkish-brown solid over the course of an hour. *N*-methylpyrrolidone (NMP, 10 mL) was added and the reaction mixture was allowed to stir overnight. The mixture was dispersed in a large volume of diethyl ether. The solid was filtered and washed several times with THF, diethyl ether, and methanol. The pinkish crude product was recrystallized from dimethylformamide (DMF), filtered, and washed with methanol to afford the pure product as a beige solid (1.22 g, 2.80 mmol, 86% isolated yield).

Alternatively, a 100 mL Erlenmeyer flask charged with a magnetic stir bar, terephthalic acid (0.543 g, 3.26 mmol), *N*-hydroxysuccinimide (NHS, 0.827 g, 7.18 mmol), and *N*-(3-dimethylaminopropyl)-*N'*-ethylcarbodiimide hydrochloride (EDC, 1.376 g, 7.18 mmol) was evacuated and backfilled with argon. DMF (25 mL) was added by syringe and the reaction mixture was allowed to react at room temperature for 24 hrs under magnetic stirring. THF (25 mL) was added by syringe and 3-aminosalicylic acid (1.50 g, 9.79 mmol) was added under positive argon pressure. Suspended solids rapidly dissolved, resulting in the formation of a dark brown solution and subsequent precipitation of a light pinkish-brown solid over the course of several hours. The reaction mixture was allowed to stir overnight. The mixture was dispersed in a large volume of diethyl ether. The solid was filtered and washed several times with THF, diethyl ether, water, and methanol. The pinkish crude product was recrystallized from dimethylformamide (DMF), filtered, and washed with methanol to afford the pure product as a beige solid (1.01 g, 2.30 mmol, 70% isolated yield).

1.2 Solution synthesis of Fe-H1

Fe(NO₃)₃·9H₂O (7.70 mg, 19.0 μmol) and ligand **H4L** (12.5 mg, 28.5 μmol) were each dissolved in DMF (1.50 mL). An aqueous solution of NaOH (4M, 30.0 μL) was added to the solution of the ligand, resulting in a color change from pinkish beige to bright yellow. The ligand solution was then added to the iron salt solution, resulting in formation of a deep red solution. The solution was allowed to sit at room temperature overnight. Formation of **Fe-H1** was confirmed by HRMS and formation of single crystals suitable for XRD studies was achieved by slow diffusion of acetone into the helicate solution (63% isolated yield based on the formula: Na₆Fe₂L₃·5DMF·3Acetone·4H₂O).

1.3 Solution synthesis of Fe-H2

Fe(NO₃)₃·9H₂O (7.70 mg, 19.0 μmol) and ligand **H4L** (12.5 mg, 28.5 μmol) were each dissolved or suspended in 2:1 EtOH:H₂O (1.25 mL). Tetrabutylammonium bromide (NEt₄Br, 36.8 mg, 175 μmol) was dissolved in DMF (500 μL) and added to the suspension of the ligand. An aqueous solution of NaOH (4M, 30.0 μL) was added to the suspension of the ligand, resulting in the immediate dissolution of the solid and formation of a bright yellow solution. The ligand solution was then added to the iron salt solution, resulting in the formation of a deep red solution. The solution was placed in a 120 °C oven overnight, resulting in precipitation of single crystals suitable for XRD studies (16% isolated yield based on the formula: Na₂(NBut₄)₄Fe₂L₃·DMF). The formation of **Fe-H2** was confirmed by HRMS.

1.4 Solution synthesis of Fe-H3

Fe(NO₃)₃·9H₂O (7.70 mg, 19.0 μmol) and ligand **H4L** (12.5 mg, 28.5 μmol) were each dissolved in DMF (1.50 mL). The ligand solution was then added to the iron salt solution, resulting in formation of a deep purple solution. An excess of N,N,N',N'-tetramethylethylenediamine (TMEDA, 100 μL) was added to the mixture, resulting in the solution going from deep purple to deep red. The solution was placed in a 120°C oven overnight. Formation of **Fe-H3** was confirmed by HRMS and the formation of single crystals suitable for XRD studies was achieved by slow diffusion of isopropanol into the helicate solution (51% isolated yield based on the formula: (H₂TMEDA)₃Fe₂L₃·DMF).

1.5 Solution synthesis of Fe-H4A

Fe(NO₃)₃·9H₂O (7.70 mg, 19.0 μmol), ligand **H4L** (12.5 mg, 28.5 μmol) and guanidinium carbonate (15.0 mg, 166 μmol) were each dissolved or suspended in H₂O (1 mL). The aqueous base solution was added to the suspension of the ligand, resulting in immediate dissolution of the solid and subsequent formation of a bright yellow suspension. The iron salt solution was then added to the ligand suspension and sonicated for 5 minutes, resulting in the formation of a deep red suspension. The reaction mixture was placed in an 70 °C oven overnight, resulting in precipitation of single crystals suitable for XRD studies (89% isolated yield based on the formula: (guanidinium)₆Fe₂L₃·7H₂O). Formation of **Fe-H4** was confirmed by HRMS.

1.6 Solution synthesis of Fe-H4B

Fe(NO₃)₃·9H₂O (7.70 mg, 19.0 μmol), ligand **H4L** (12.5 mg, 28.5 μmol) and guanidinium carbonate (15.0 mg, 166 μmol) were each dissolved or suspended in H₂O (1 mL). The aqueous base solution was added to the suspension of the ligand, resulting in immediate dissolution of the solid and subsequent formation of a bright yellow suspension. The iron salt solution was then added to the ligand suspension and sonicated for 5 minutes, resulting in the formation of a deep red suspension. The reaction mixture was placed in an

85 °C oven overnight, resulting in the precipitation of single crystals suitable for XRD studies (89% isolated yield based on the formula: (guanidinium)₆Fe₂L₃·4H₂O).

1.7 Solution synthesis of Fe-H4C

Fe(NO₃)₃·9H₂O (7.70 mg, 19.0 μmol), ligand **1** (12.5 mg, 28.5 μmol) and guanidinium carbonate (15.0 mg, 166 μmol) were each dissolved or suspended in H₂O (1 mL). The aqueous base solution was added to the suspension of the ligand, resulting in immediate dissolution of the solid and subsequent formation of a bright yellow suspension. The iron salt solution was then added to the ligand suspension and manually stirred for 15 min, resulting in the formation of a deep red suspension. The reaction mixture was filtered and **Fe-H4C** characterized by PXRD. Upon standing in solution or as a filtered solid, **Fe-H4C** converts to **Fe-H4A** (see Fig. S18).

1.8 Solution synthesis of Cu-H1

Cu(OTf)₂ (10.2 mg, 28.5 μmol) and ligand **H4L** (12.5 mg, 28.5 μmol) were each dissolved or suspended in 9:1 *i*PrOH/DMF (1.50 mL). An aqueous solution of NaOH (4M, 30.0 μL) was added to the suspension of the ligand, resulting in immediate dissolution of the solid and formation of a bright yellow solution. The ligand solution was then added to the copper salt solution, resulting in the formation of a deep green solution. The solution was placed in a 120 °C oven overnight, resulting in the precipitation of single crystals suitable for XRD studies (34% isolated yield based on the formula: Na₄Cu₂L₂·3DMF). Formation of **Cu-H1** was confirmed by HRMS.

1.9 Solution synthesis of Cu-H2

Cu(OTf)₂ (10.2 mg, 28.5 μmol) and **H4L** (12.5 mg, 28.5 μmol) were each dissolved or suspended in *i*PrOH (1.50 mL). Guanidinium carbonate (15.0 mg, 166 μmol) was dissolved in H₂O (250 μL). The aqueous base solution was added to the suspension of the ligand, resulting in immediate dissolution of the solid and formation of a bright yellow solution. The ligand solution was then added to the copper salt solution, resulting in formation of a deep green solution and formation of a precipitate within a few minutes. The solution was placed in an 80°C oven overnight, resulting in the appearance of single crystals suitable for single crystal X-ray diffraction studies (93% isolated yield based on the formula: (guanidinium)₄Cu₂L₂·H₂O·*i*PrOH). Formation of **Cu-H2** was confirmed by HRMS.

1.10 General procedure for the mechanochemical synthesis of helicates

All milling procedures were conducted in a 5 mL volume stainless steel milling jar charged with a single stainless steel ball bearing (7 mm diameter, 0.7 g). Materials were loaded into the milling jar and liquid additive was added. The jar was then loaded onto a Retsch MM200 mill operating at a frequency of 25 Hz for 30 min. Liquid additives were chosen based on the solvent initially used to conduct solution reactions or from which the helicates were crystallized.

1.11 Mechanochemical synthesis of Fe-H1

Fe(NO₃)₃·9H₂O (31.0 mg, 76.0 μmol), ligand **H4L** (50.0 mg, 114 μmol), and Na₂CO₃ (50.0 mg, 471 μmol) were loaded into the milling jar. DMF (50 μL, $\eta = 0.38 \mu\text{L}/\text{mg}$) was added as a liquid additive and the reaction mixture was milled for 30 min. Formation of **Fe-H1** was confirmed by HRMS and PXRD.

1.12 Mechanochemical synthesis of Fe-H2

Fe(NO₃)₃·9H₂O (20.7 mg, 50.7 μmol), ligand **H4L** (33.3 mg, 76.0 μmol), Na₂CO₃ (33.3 mg, 314 μmol), and (NEt₄Br, 61.7 mg, 293 μmol) were loaded into the milling jar. DMF (56 μL, $\eta = 0.38 \mu\text{L}/\text{mg}$) was added as a liquid additive and the reaction mixture was milled for 30 min. Formation of **Fe-H2** was confirmed by HRMS and PXRD.

1.13 Mechanochemical synthesis of Fe-H3

Fe(NO₃)₃·9H₂O (46.5 mg, 114 μmol), ligand **H4L** (75.0 mg, 171 μmol), and TMEDA (51 μL, 342 μmol) were loaded into the milling jar. DMF (70.0 μL, $\eta = 0.38 \mu\text{L}/\text{mg}$) was added as a liquid additive and the reaction mixture was milled for 30 min. Formation of **Fe-H3** was confirmed by HRMS and PXRD.

1.14 Mechanochemical synthesis of Fe-H4A

Fe(NO₃)₃·9H₂O (31.0 mg, 76.0 μmol), ligand **H4L** (50.0 mg, 114 μmol), and guanidinium carbonate (41.0 mg, 456 μmol) were loaded into the milling jar. MeNO₂ or MeCN (61 μL, $\eta = 0.50 \mu\text{L}/\text{mg}$) was added as a liquid additive and the reaction mixture was milled for 30 min. Formation of **Fe-H4** was confirmed by HRMS and PXRD.

1.15 Mechanochemical synthesis of Fe-H4C

Fe(NO₃)₃·9H₂O (31.0 mg, 76.0 μmol), ligand **H4L** (50.0 mg, 114 μmol), and guanidinium carbonate (41.0 mg, 456 μmol) were loaded into the milling jar. H₂O (45 μL, $\eta = 0.38 \mu\text{L}/\text{mg}$) was added as a liquid additive and the reaction mixture was milled for 30 min. Formation of **Fe-H4C** was confirmed by PXRD.

1.16 Mechanochemical synthesis of Cu-H1

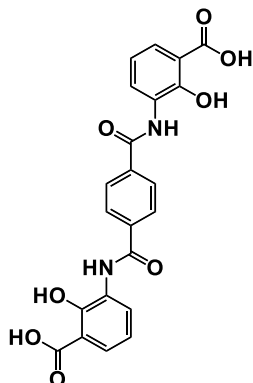
Cu(OTf)₂ (41.0 mg, 114 μmol), ligand **H4L** (50.0 mg, μmol), and Na₂CO₃ (50.0 mg, 431 μmol) were loaded into the milling jar. DMF (50 μL, $\eta = 0.35 \mu\text{L}/\text{mg}$) was added as a liquid additive and the reaction mixture was milled for 30 min. Formation of **Cu-H1** was confirmed by HRMS.

1.17 Mechanochemical synthesis of Cu-H2

Cu(OTf)₂ (41.0 mg, 114 μmol), ligand **H4L** (50.0 mg, μmol), and guanidinium carbonate (30.0 mg, 333 μmol) were loaded into the milling jar. An optimized mixture of 9:1 *i*PrOH/H₂O (50 μL, $\eta = 0.41 \mu\text{L}/\text{mg}$) was added as a liquid additive and the reaction mixture was milled for 30 min. Formation of **Cu-H2** was confirmed by HRMS and PXRD. For the synthesis of **Cu-H2** from CuO, CuO (20.0 mg, 250 μmol), ligand **1** (110.0 mg, 250 μmol), and NH₄OAc (2.0 mg, 25 μmol, 10 mol %) were loaded into the milling jar and the reaction mixture was milled for 90 min. Guanidinium carbonate (55.0 mg, 611 μmol) and a mixture of 9:1 *i*PrOH/H₂O (75 μL, $\eta = 0.42 \mu\text{L}/\text{mg}$) was added as a liquid additive and the reaction mixture was milled. Formation of **Cu-H2** was confirmed by HRMS and PXRD.

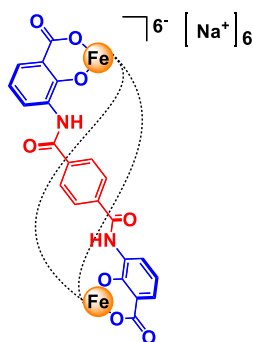
2. Summary of IR, ¹H and ¹³C NMR and HR-MS Data

N,N'-bis(3-carboxy-2-hydroxyphenyl)terephthalamide (H4L)



Beige to pinkish-brown solid (86% yield); **IR** (ν , cm^{-1}) 557, 627, 654, 721, 755, 843, 859, 895, 1079, 1123, 1185, 1245, 1314, 1339, 1435, 1460, 1505, 1538, 1612, 1643, 3314, 2600-3200 (broad) **¹H-NMR** (300 MHz, DMSO-*d*₆) δ 6.90-7.00 (t, J = 8 Hz, 2H), δ 7.64-7.73 (dd, J = 8, 1.6 Hz, 2H), δ 7.86-7.97 (dd, J = 8, 1.5 Hz, 2H), δ 8.10 (s, 4H), δ 9.82 (s, 2H) **¹³C-NMR** (500 MHz, DMSO-*d*₆) δ 113.65, δ 118.91, δ 126.76, δ 127.33, δ 128.24, δ 131.48, δ 137.34, δ 155.13, δ 165.08, δ 172.66 **HR-MS**: calculated for C₂₂H₁₆N₂O₈ [M]: 436.09; measured m/z C₂₂H₁₆N₂O₈ [M – H]: 435.08

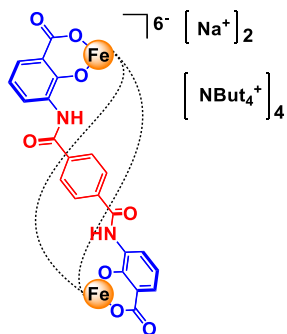
Fe-H1



Bright red solid and dark red crystals; **IR** (ν , cm^{-1}) 585, 661, 758, 867, 1063, 1102, 1229, 1254, 1354, 1389, 1432, 1496, 1524, 1647, 3046-3720

HR-MS for Fe-H1			
Formula	Calculated m/z	Measured m/z (solution)	Measure m/z (solid-state)
C ₆₆ H ₃₆ Fe ₂ N ₆ O ₂₄ Na ₆ [M]	1545.99	-	-
C ₆₆ H ₄₀ Fe ₂ N ₆ O ₂₄ [M – 6Na + 4H]	706.04	706.04	-
C ₆₆ H ₃₈ Fe ₂ N ₆ O ₂₄ [M – 6Na + 2H]	352.52	-	352.52

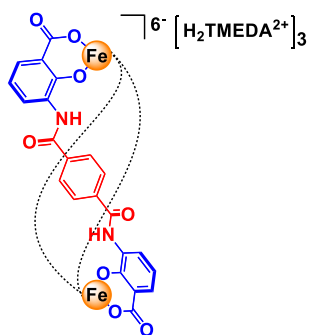
Fe-H2



Bright red solid and dark red crystals; **IR** (ν , cm^{-1}) 558, 590, 638, 714, 731, 751, 795, 841, 860, 892, 940, 1068, 1128, 1190, 1284, 1349, 1392, 1435, 1485, 1503, 1539, 1602, 1632, 1658, 3397

HR-MS for Fe-H2			
Formula	Calculated m/z	Measured m/z (solution)	Measure m/z (solid-state)
$\text{C}_{130}\text{H}_{180}\text{Fe}_2\text{N}_{10}\text{O}_{24}\text{Na}_2$ [M]	2423.17	-	-
$\text{C}_{130}\text{H}_{180}\text{Fe}_2\text{N}_{10}\text{O}_{24}$ [M - 2Na]	1188.60	1189.10	-
$\text{C}_{114}\text{H}_{144}\text{Fe}_2\text{N}_9\text{O}_{24}$ [M - 2Na - NBut ₄]	711.63	711.97	-
$\text{C}_{114}\text{H}_{145}\text{Fe}_2\text{N}_9\text{O}_{24}$ [M - 2Na - NBut ₄ + 1H]	1067.96	1068.46	-
$\text{C}_{66}\text{H}_{38}\text{Fe}_2\text{N}_6\text{O}_{24}$ [M - 2Na - 4NBut ₄ + 2H]	352.52	-	352.52

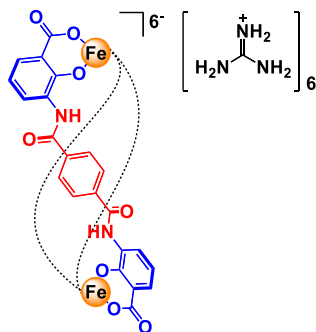
Fe-H3



Bright red solid and dark red crystals; **IR** (ν , cm^{-1}) 507, 581, 659, 758, 816, 860, 893, 953, 1090, 1162, 1191, 1226, 1254, 1349, 1386, 1428, 1471, 1490, 1520, 1602, 1652, 2969, 3140-3670 (broad)

HR-MS for Fe-H3			
Formula	Calculated m/z	Measured m/z (solution)	Measure m/z (solid-state)
$\text{C}_{84}\text{H}_{90}\text{Fe}_2\text{N}_{12}\text{O}_{24}$ [M]	1762.49	-	-
$\text{C}_{66}\text{H}_{40}\text{Fe}_2\text{N}_6\text{O}_{24}$ [M - 3TMEDA + 4H]	706.04	706.04	706.04

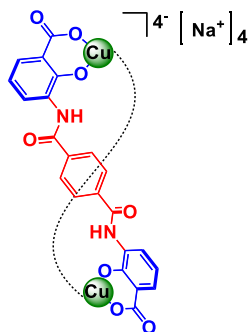
Fe-H4



Bright red solid and dark red crystals; **IR** (ν , cm^{-1}) **Fe-H4A** 583, 641, 722, 761, 812, 860, 893, 949, 1017, 1081, 1155, 1191, 1233, 1343, 1426, 1468, 1515, 1600, 1645, 2874-3707 (broad) **Fe-H4B** 553, 584, 639, 661, 722, 760, 803, 862, 892, 950, 1013, 1075, 1150, 1194, 1235, 1342, 1424, 1467, 1496, 1515, 1600, 1649, 2887-3220 (broad), 3220-3497 (broad)

HR-MS for Fe-H4			
Formula	Calculated m/z	Measured m/z (solution)	Measure m/z (solid-state)
$\text{C}_{72}\text{H}_{72}\text{Fe}_2\text{N}_{24}\text{O}_{24}$ [M]	1769.14	-	-
$\text{C}_{67}\text{H}_{44}\text{Fe}_2\text{N}_9\text{O}_{24}$ [M - 5Gua + 2H]	490.04	488.00	-
$\text{C}_{66}\text{H}_{38}\text{Fe}_2\text{N}_6\text{O}_{24}$ [M - 6Gua + 2H]	352.52	352.52	353.20
$\text{C}_{66}\text{H}_{40}\text{Fe}_2\text{N}_6\text{O}_{24}$ [M - 6Gua + 4H]	706.04	-	706.04

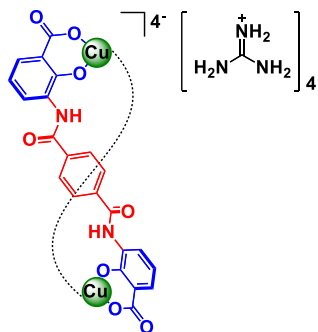
Cu-H1



Dark green solid and dark green crystals; **IR** (ν , cm^{-1}) 517, 584, 639, 660, 707, 757, 865, 895, 953, 1032, 1063, 1096, 1156, 1225, 1255, 1353, 1388, 1412, 1436, 1495, 1652, 2831-2900 (broad), 2900-3037 (broad), 3108-3690 (broad)

HR-MS for Cu-H1			
Formula	Calculated m/z	Measured m/z (solution)	Measure m/z (solid-state)
$\text{C}_{44}\text{H}_{24}\text{Cu}_2\text{N}_4\text{O}_{16}\text{Na}_4$ [M]	1081.94	-	-
$\text{C}_{44}\text{H}_{24}\text{Cu}_2\text{N}_4\text{O}_{16}\text{Na}_2$ [M - 2Na]	517.98	517.98	517.98
$\text{C}_{44}\text{H}_{24}\text{Cu}_2\text{N}_4\text{O}_{16}\text{Na}_1$ [M - 3Na]	337.66	-	338.32

Cu-H2



Dark green solid and dark green crystals; **IR** (ν , cm^{-1}) 581, 635, 680, 747, 816, 861, 896, 955, 1008, 1072, 1155, 1186, 1256, 1349, 1398, 1428, 1468, 1495, 1520, 1601, 1652, 2870-3242 (broad), 3242-3515 (broad)

HR-MS for Cu-H1			
Formula	Calculated m/z	Measured m/z (solution)	Measure m/z (solid-state)
$C_{48}H_{48}Cu_2N_{16}O_{16}$ [M]	1230.20	-	-
$C_{44}H_{26}Cu_2N_4O_{16}$ [M - 4 Gua + 2H]	496.00	496.00	496.00 (triflate) 496.00 (oxide)

3. ^1H and ^{13}C -NMR Spectra

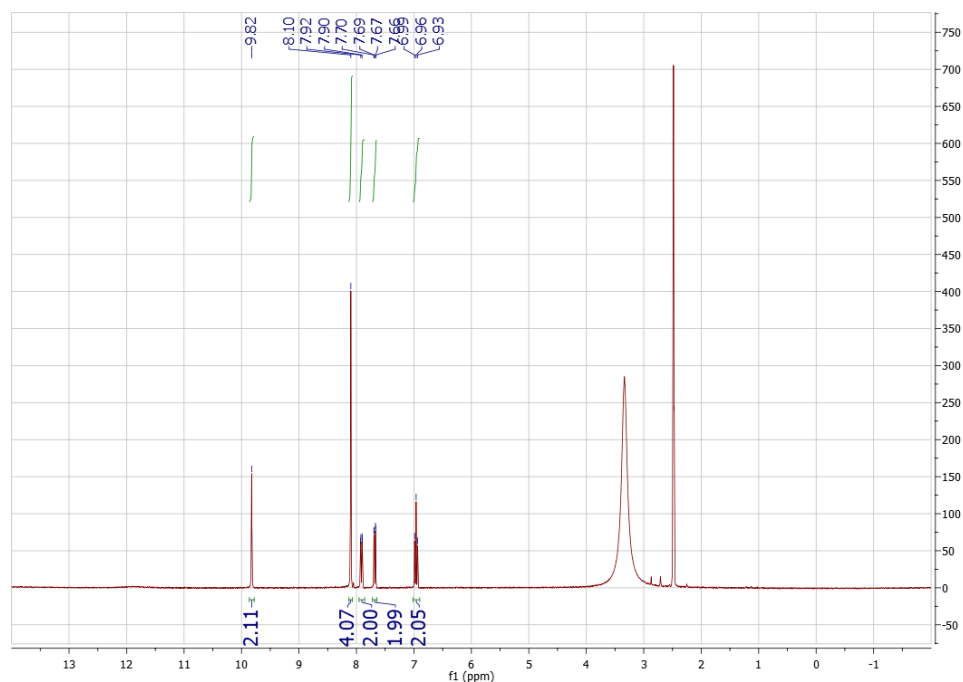


Figure S1. ^1H -NMR spectrum of H4L made from terephthaloyl chloride

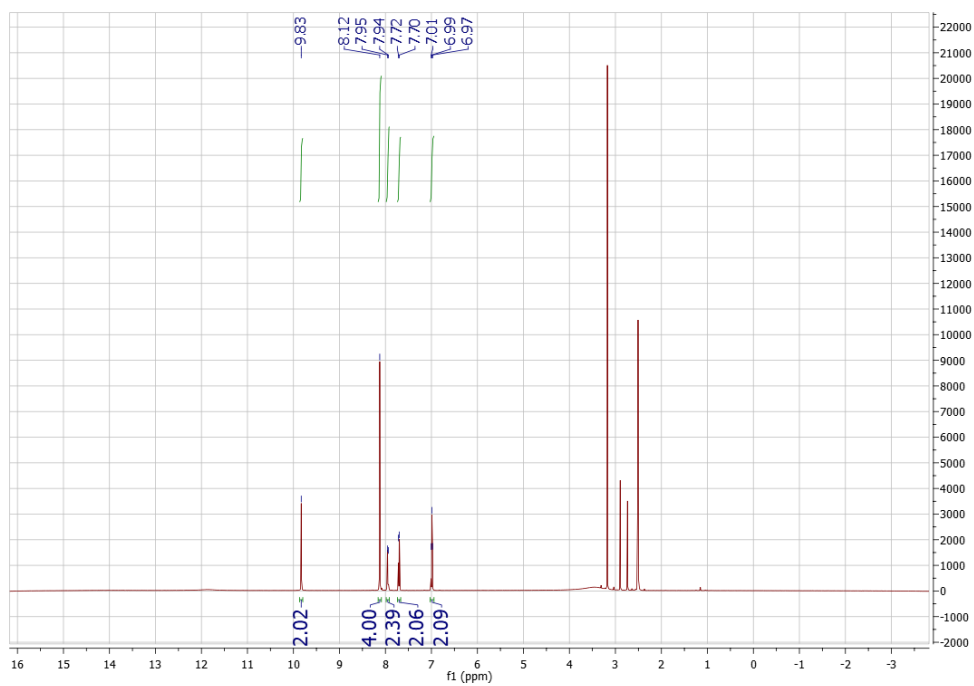


Figure S2. $^1\text{H-NMR}$ spectrum of H_4L made from terephthalic acid



Figure S3. $^{13}\text{C-NMR}$ spectrum of H_4L made from terephthaloyl chloride

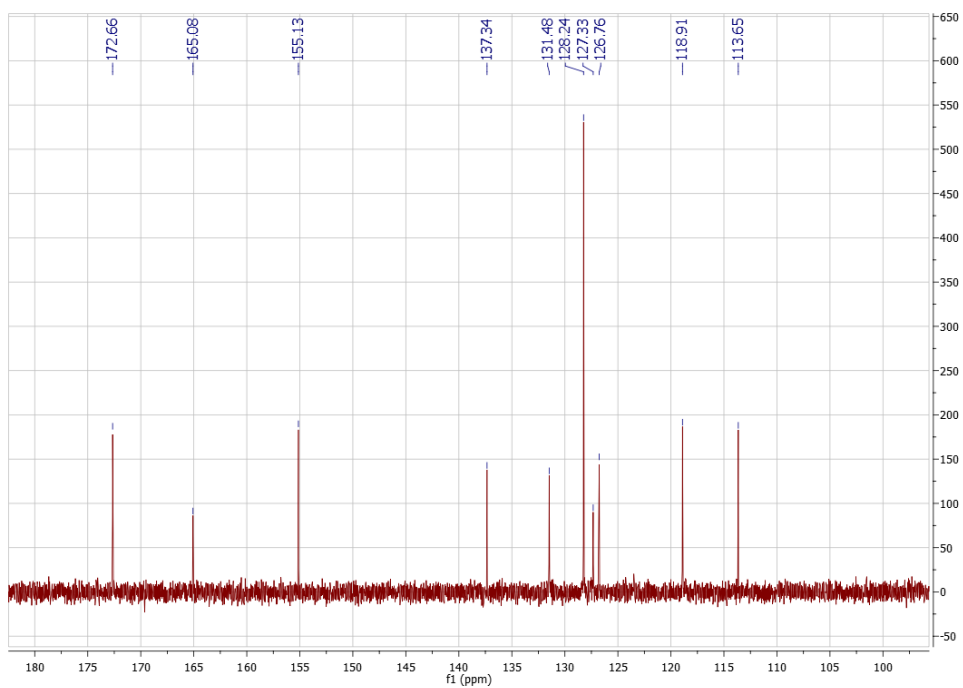


Figure S4. ^{13}C -NMR spectrum of H_4L made from terephthalic acid

4. Fourier-Transform Attenuated Total Reflectance (FTIR-ATR) Spectra

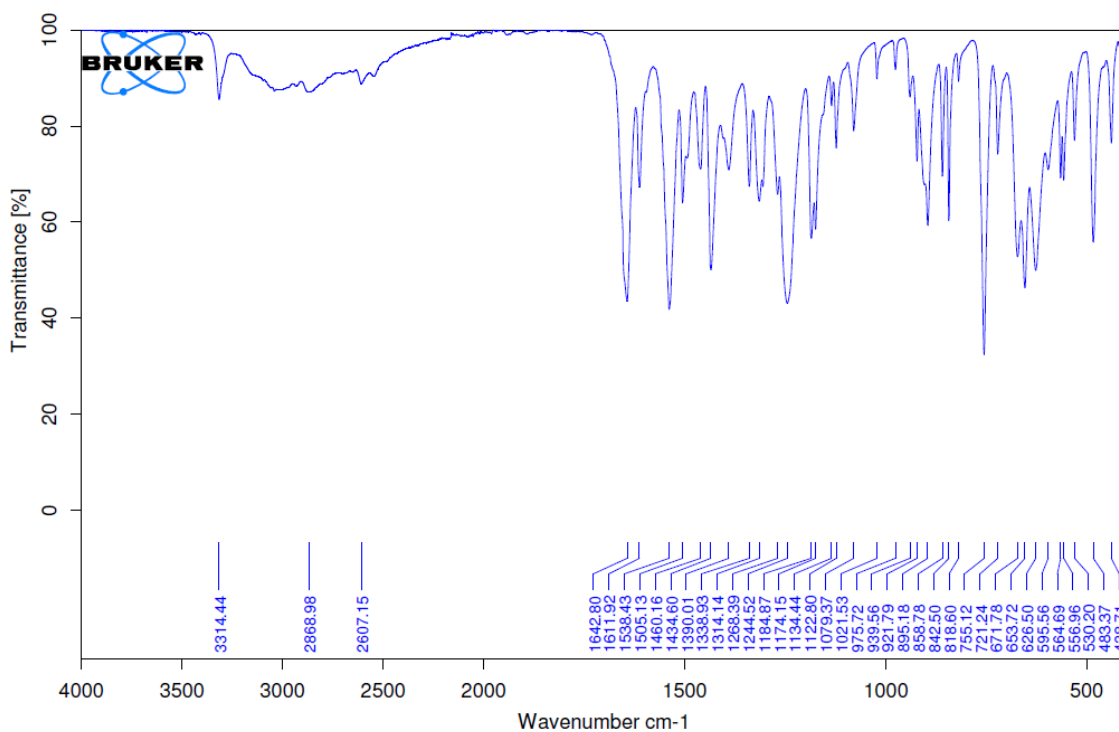


Figure S5. FTIR-ATR spectrum of H_4L .

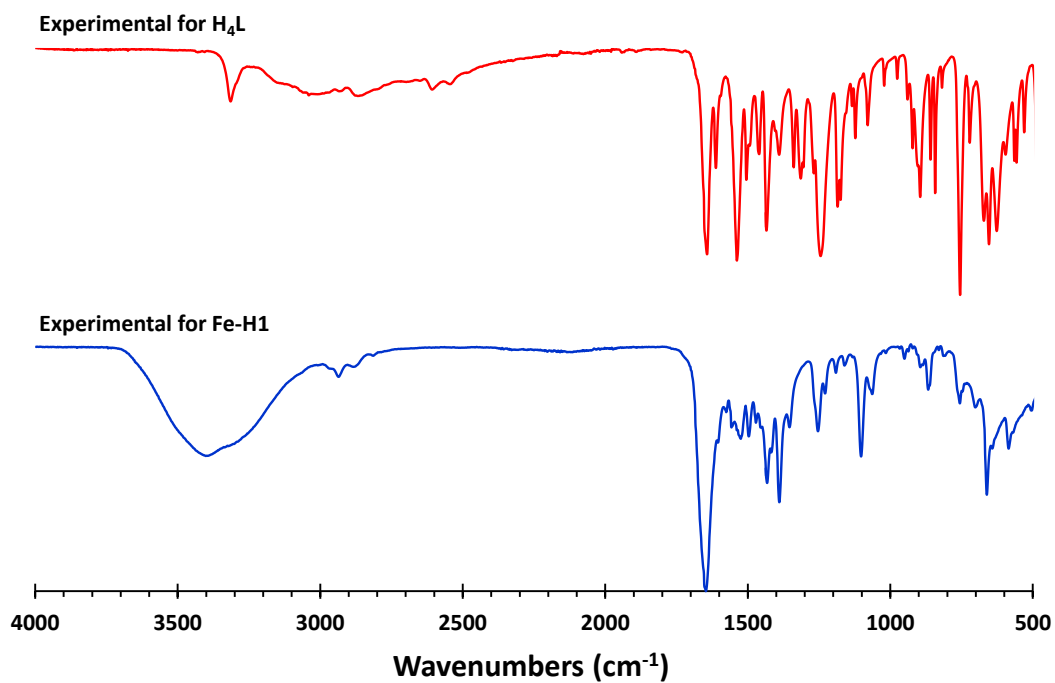
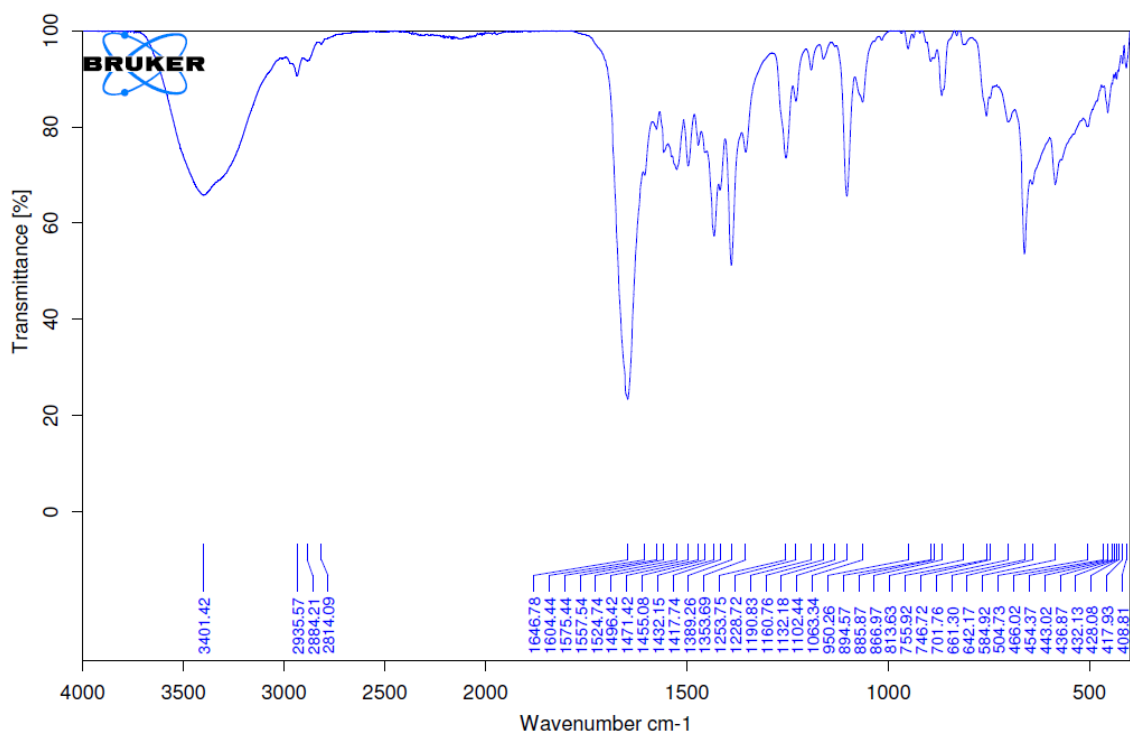


Figure S6. FTIR-ATR spectra of **Fe-H1** (top) and stacked for comparison with ligand (bottom)

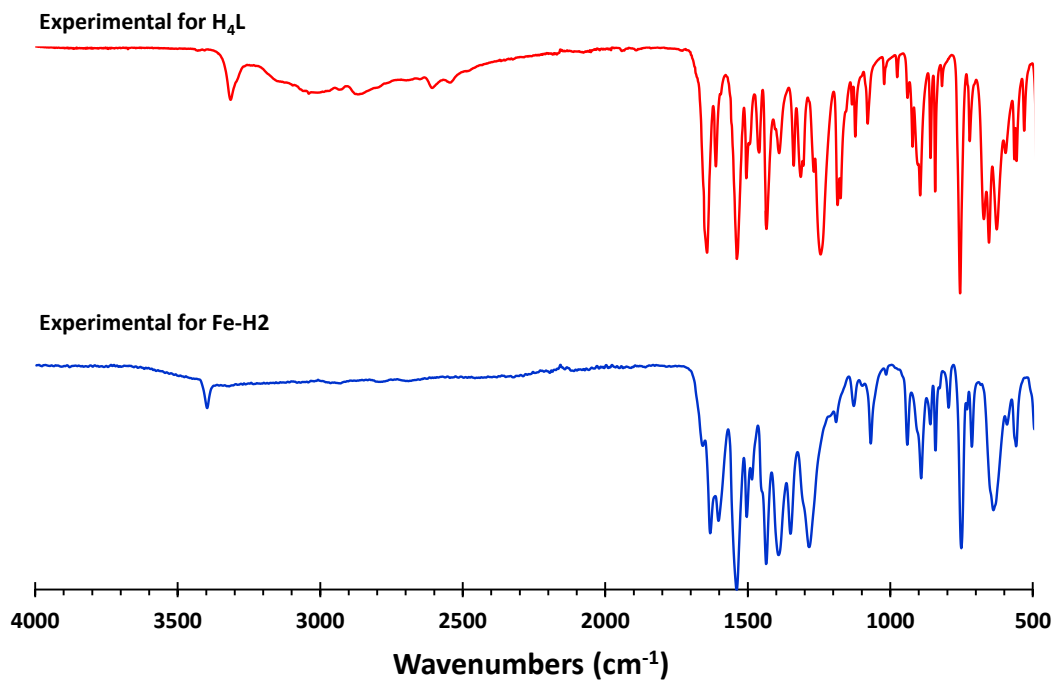
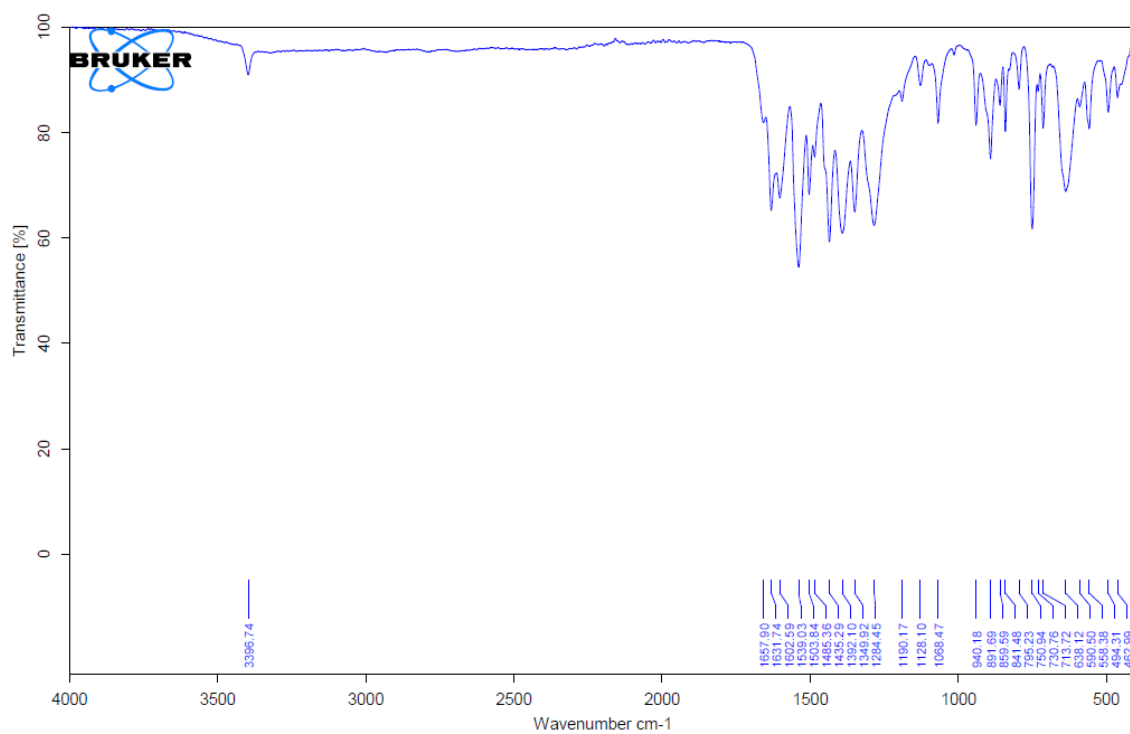


Figure S7. FTIR-ATR spectrum of Fe-H2 and stacked for comparison with ligand (bottom)

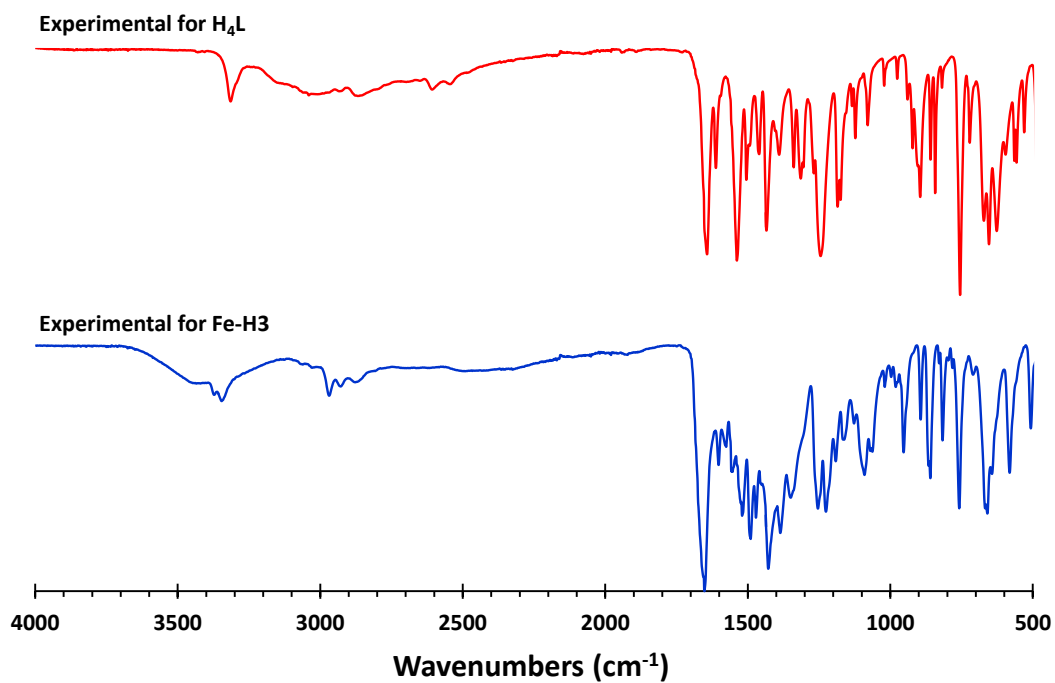
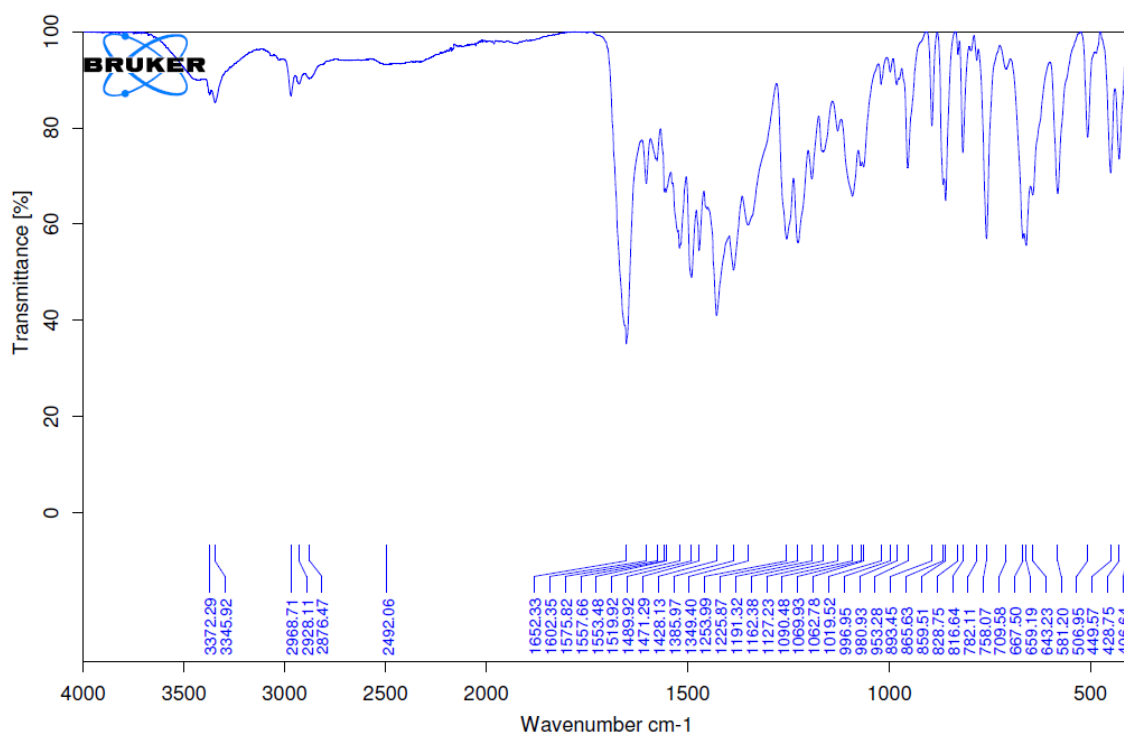


Figure S8. FTIR-ATR spectrum of **Fe-H3** and stacked for comparison with ligand (bottom)

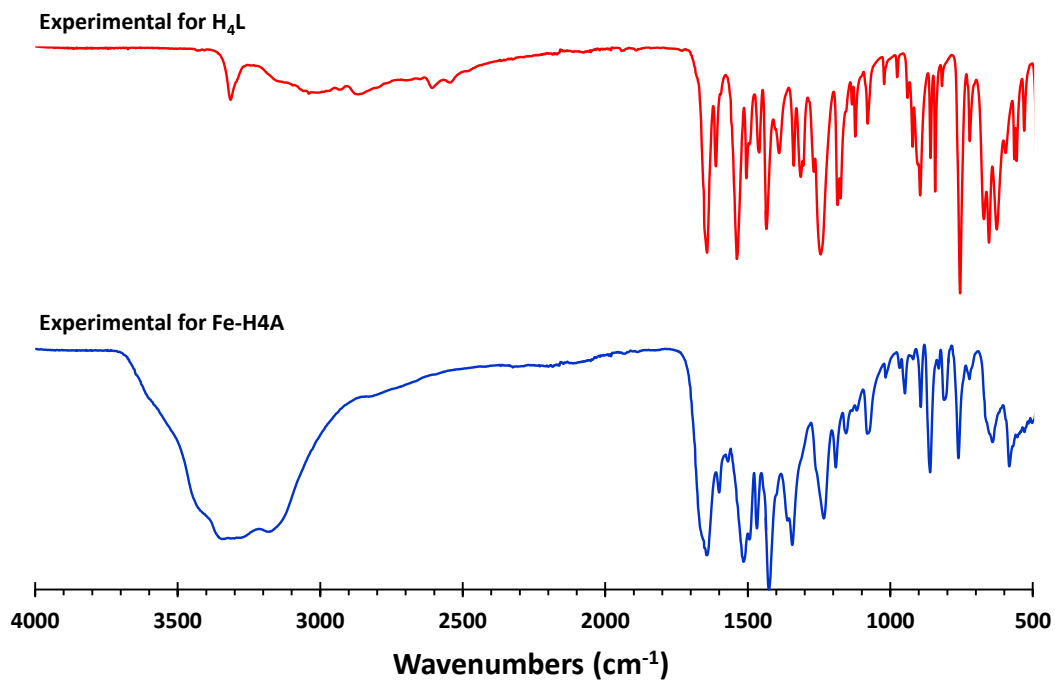
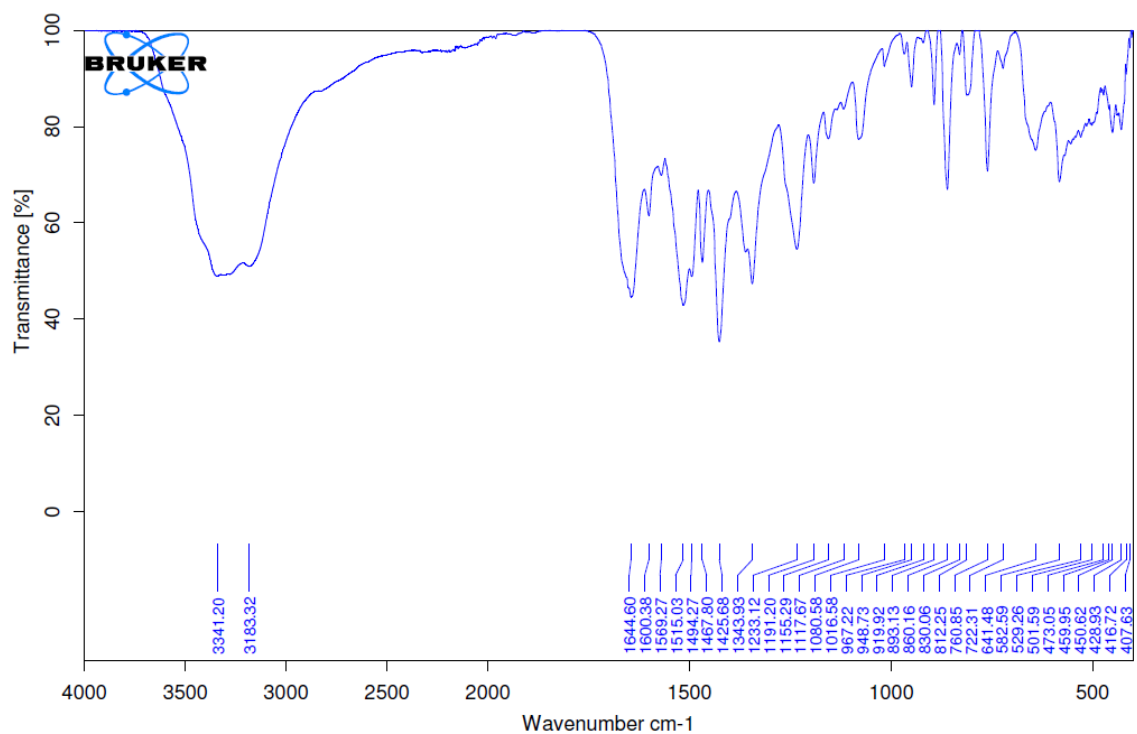


Figure S9. FTIR-ATR spectrum of **Fe-H4A** and stacked for comparison with ligand (bottom)

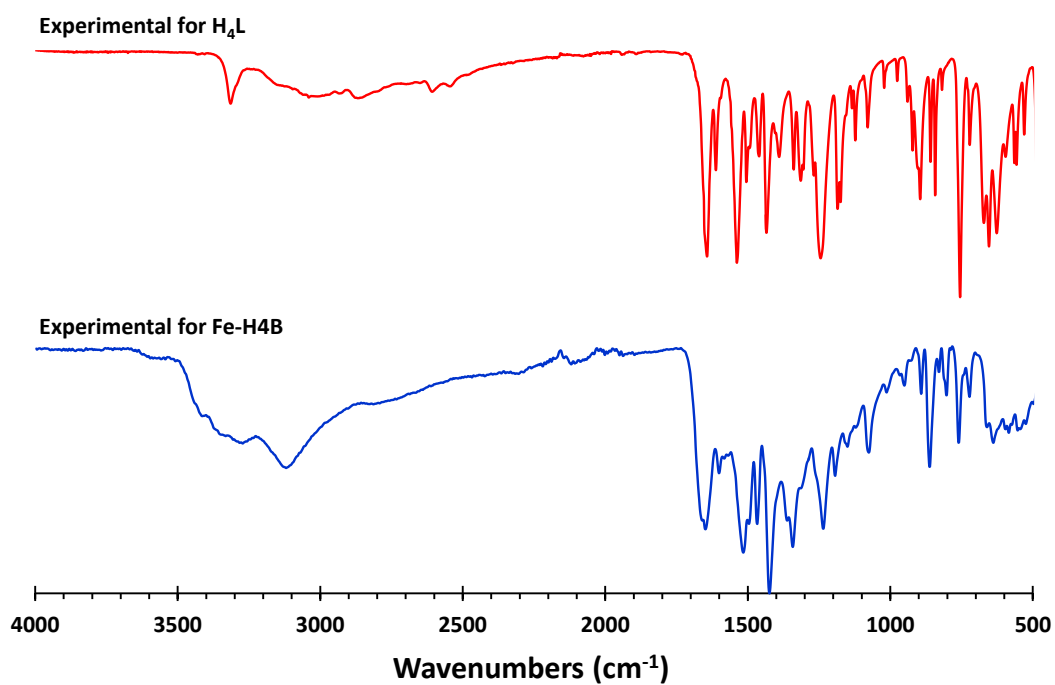
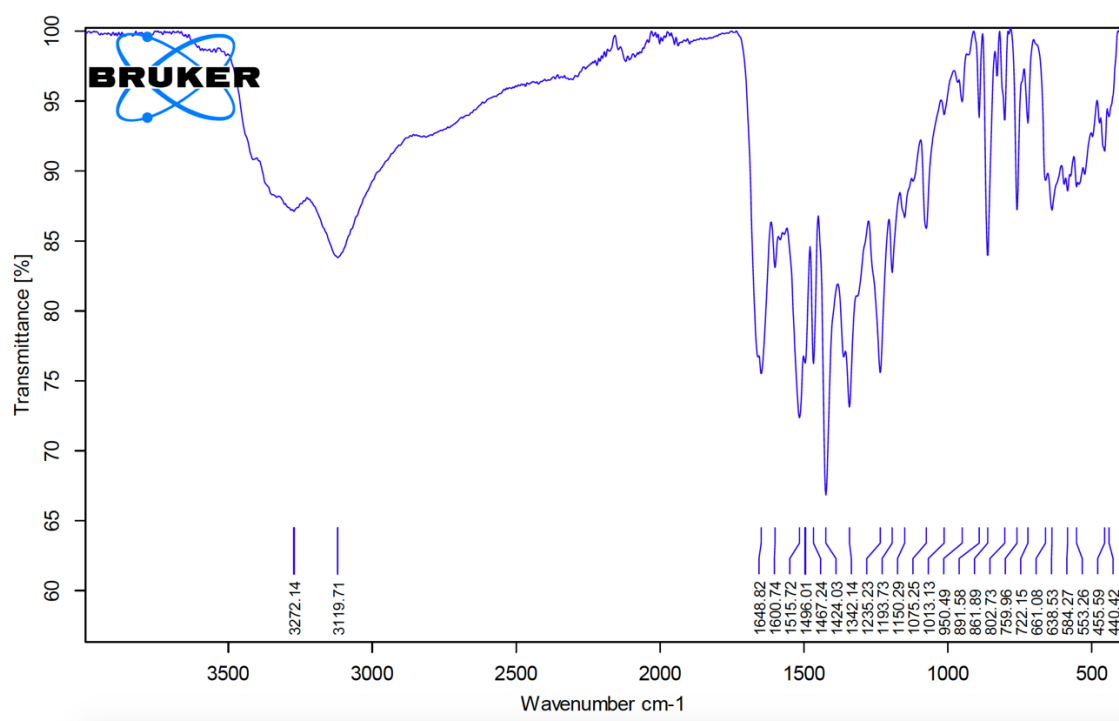


Figure S10. FTIR-ATR spectrum of **Fe-H4B** and stacked for comparison with ligand (bottom)

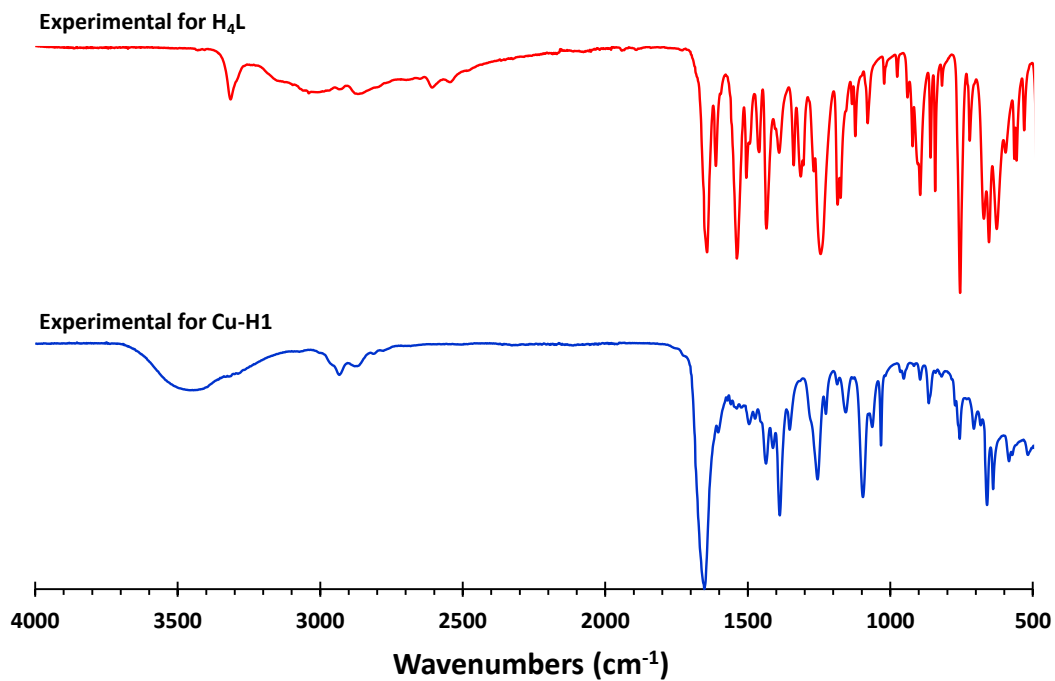
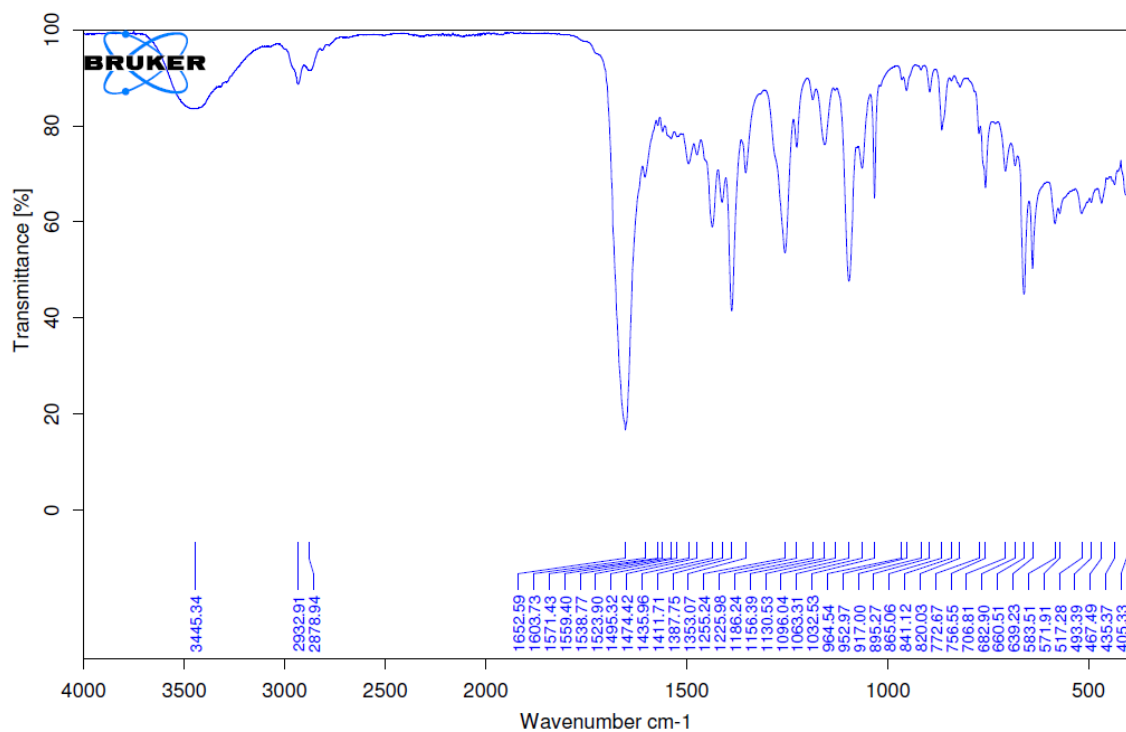


Figure S11. FTIR-ATR spectrum of **Cu-H1** and stacked for comparison with ligand (bottom)

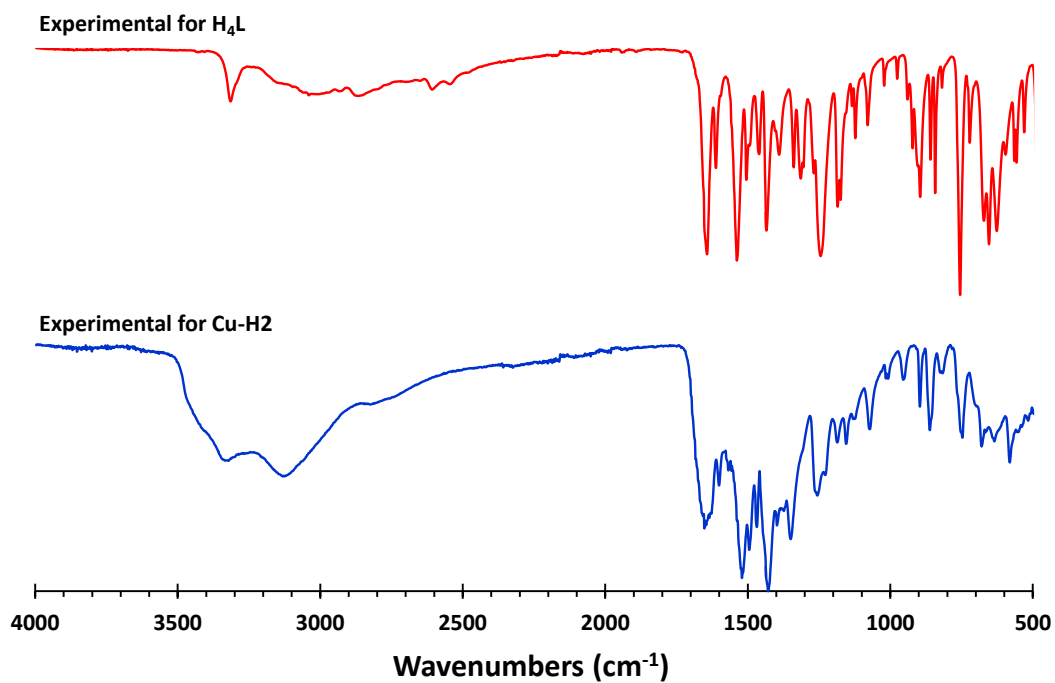
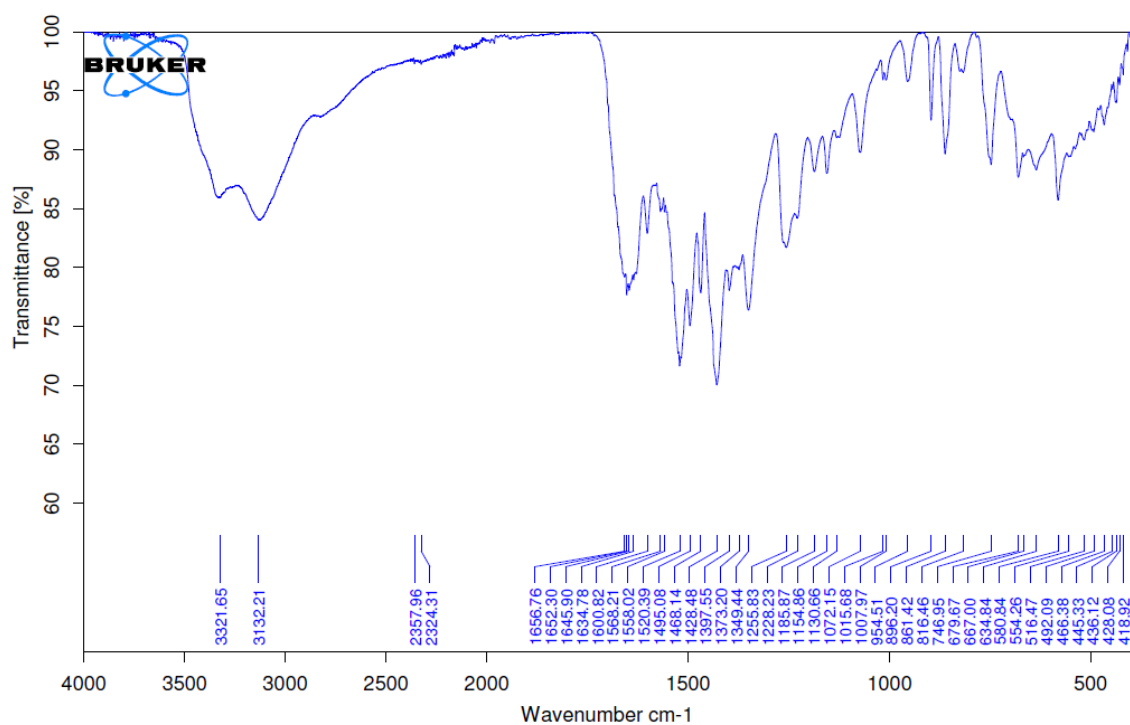


Figure S12. FTIR-ATR spectrum of **Cu-H2** and stacked for comparison with ligand (bottom)

5. Powder X-Ray Diffraction (PXRD) Patterns

Simulated PXRD patterns from single crystal data are shown as red colored patterns. The PXRD patterns of materials obtained from solution are shown in black, orange, and gold. The PXRD patterns of mechanochemically obtained materials are shown in blue, green, and purple.

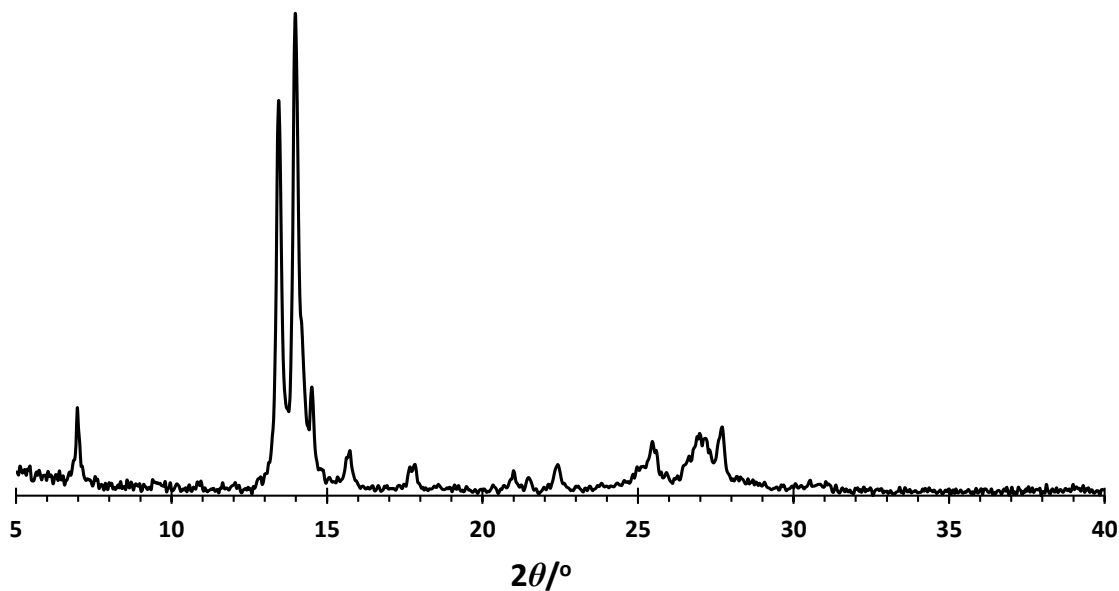


Figure S13. Experimentally acquired PXRD pattern of H₄L.

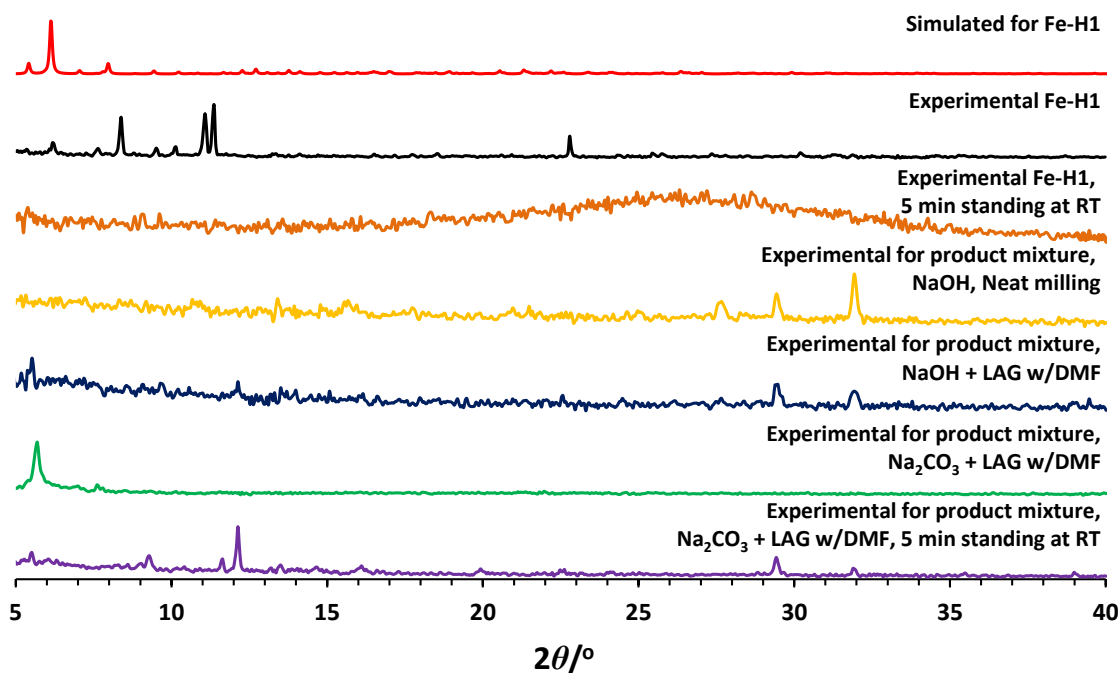


Figure S14. Simulated and experimentally acquired PXRD pattern of Fe-H1.

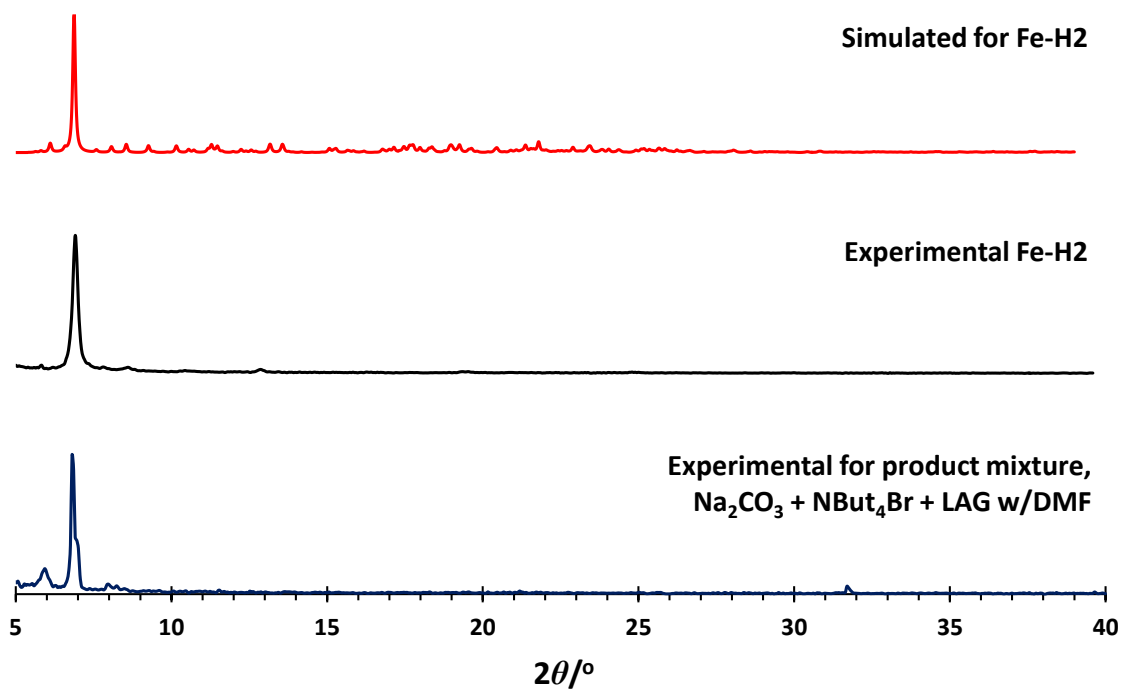


Figure S15. Simulated and experimentally acquired PXRD pattern of **Fe-H2**.

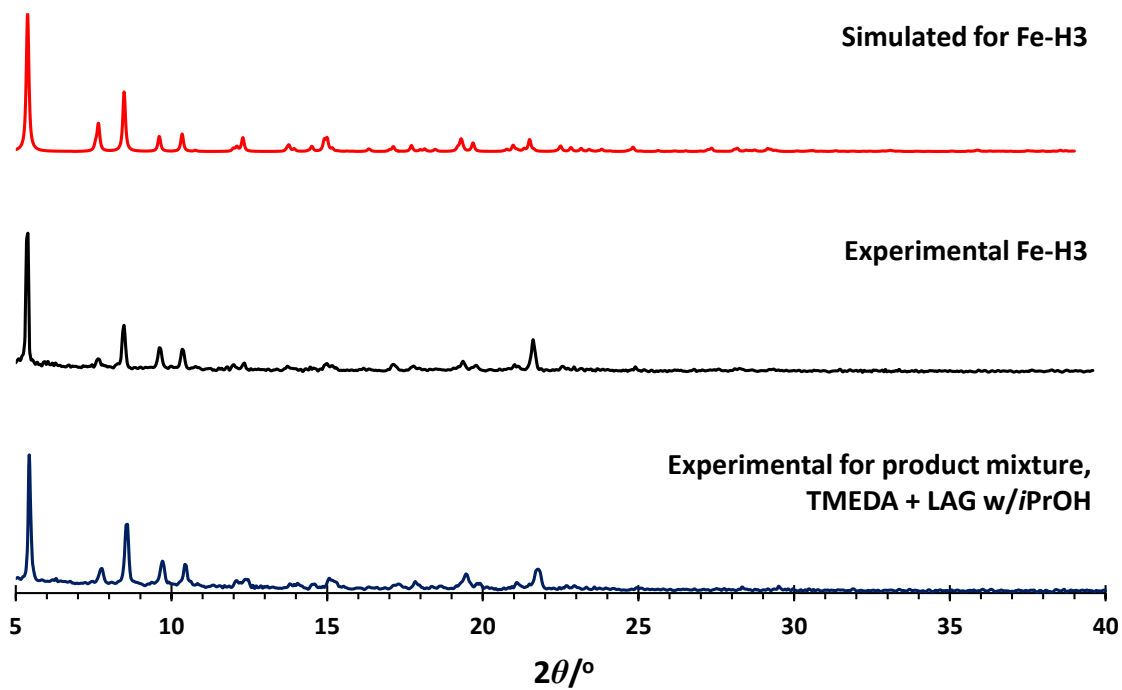


Figure S16. Simulated and experimentally acquired PXRD pattern of **Fe-H3**.

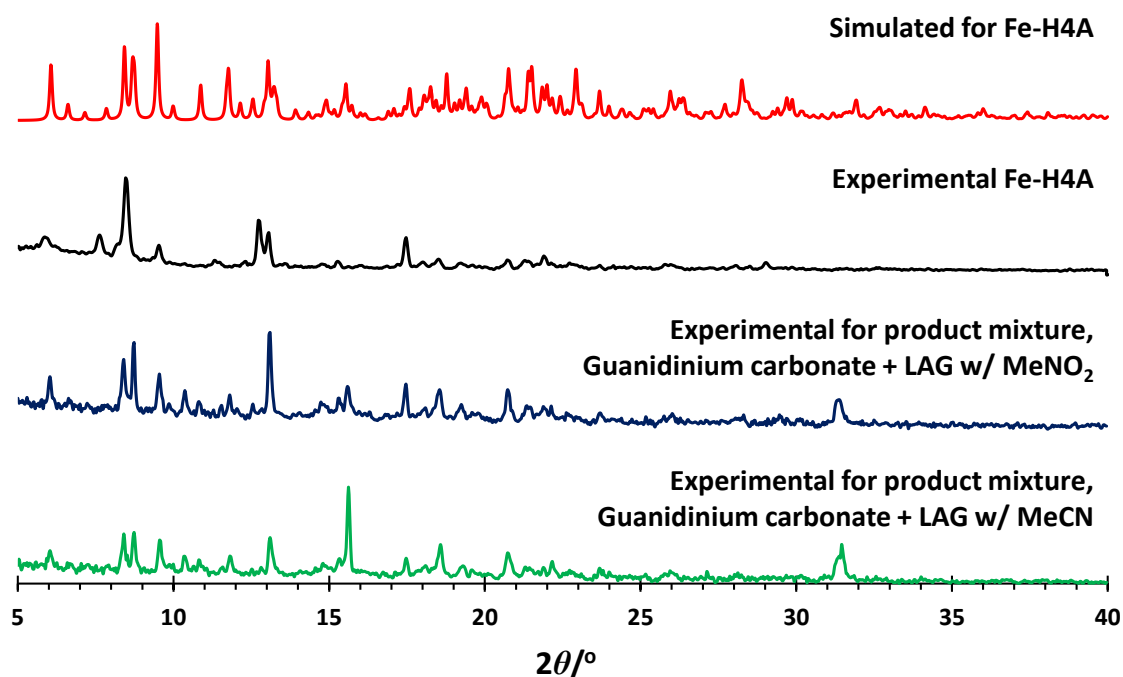


Figure S17. Simulated and experimentally acquired PXRD pattern of **Fe-H4A**.

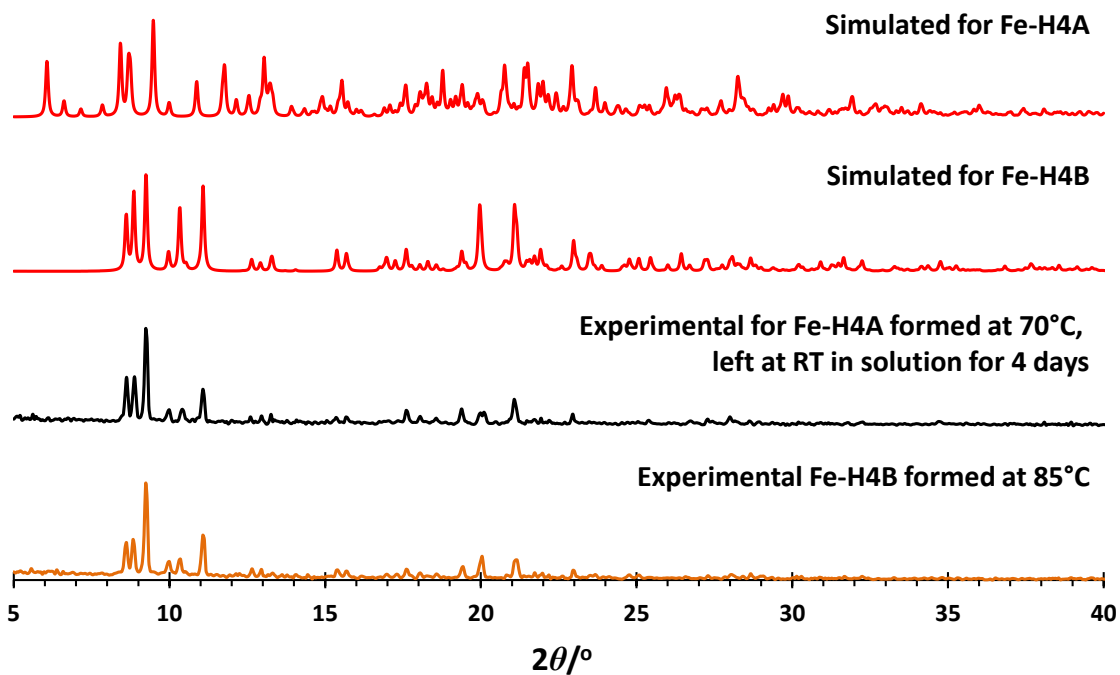


Figure S18. Simulated and experimentally acquired PXRD pattern of **Fe-H4B**, demonstrating conversion of **Fe-H4A** to **Fe-H4B** upon standing in solution.

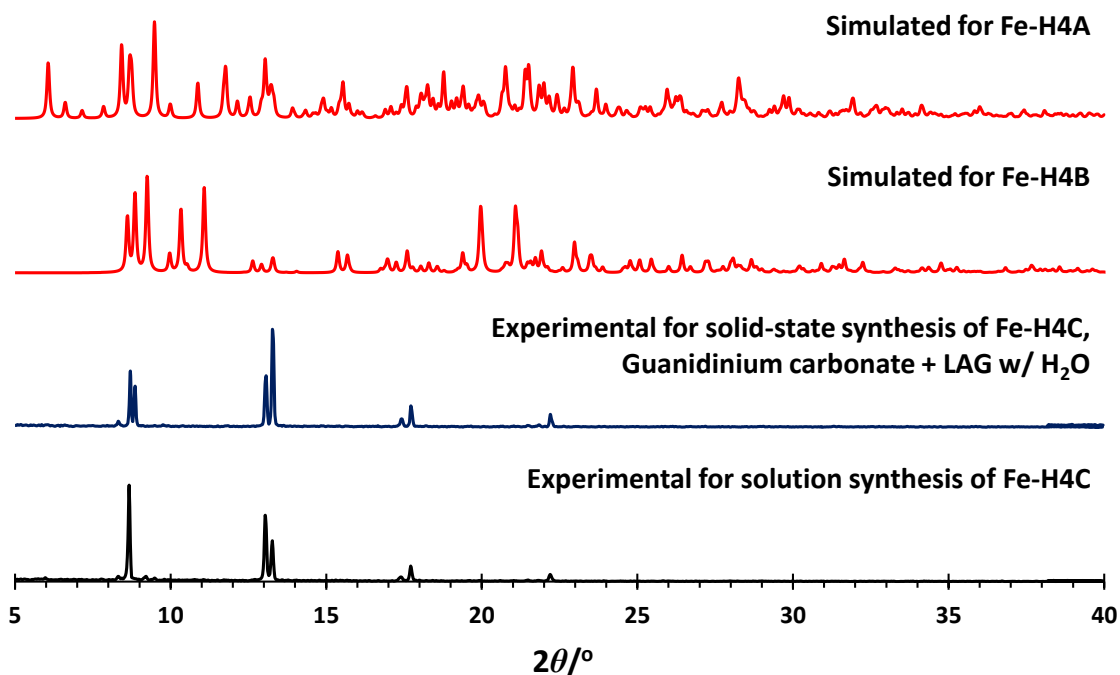


Figure S19. Comparison of simulated PXRD pattern of **Fe-H4A**, **Fe-H4B**, and experimental PXRD patterns of **Fe-H4C** acquired mechanochemically and from solution.

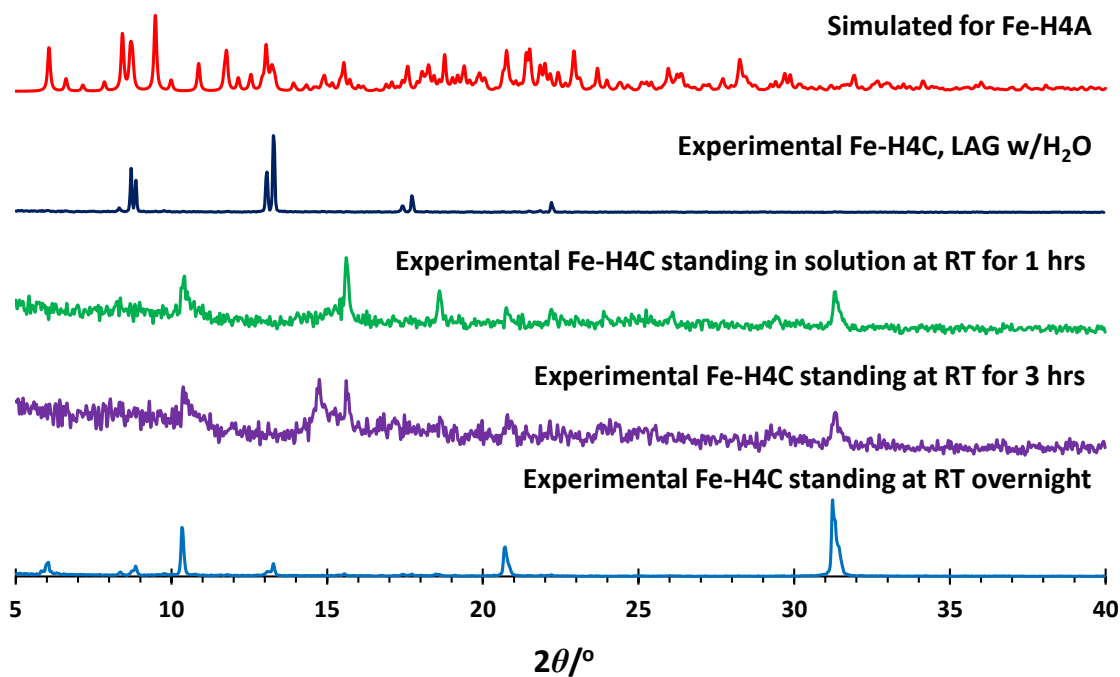


Figure S20. Comparison of simulated PXRD pattern of **Fe-H4A**, experimental PXRD patterns of **Fe-H4C** acquired mechanochemically, and **Fe-H4C** upon standing at room temperature, showing conversion to **Fe-H4A**.

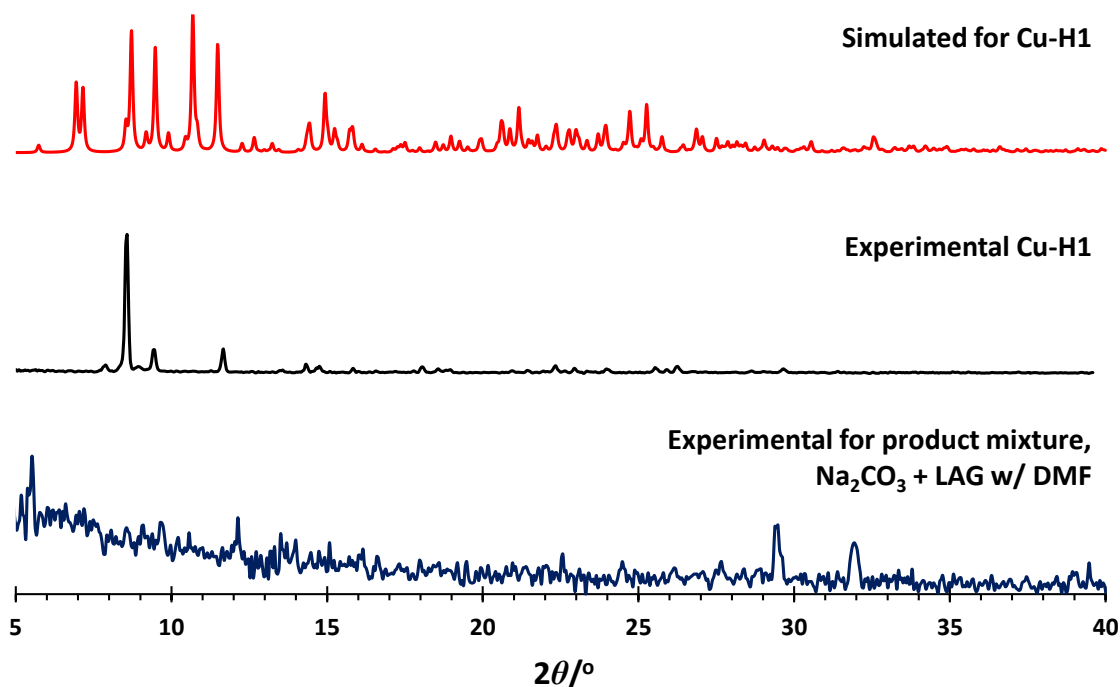


Figure S21. Simulated and experimentally acquired PXRD pattern of **Cu-H1**

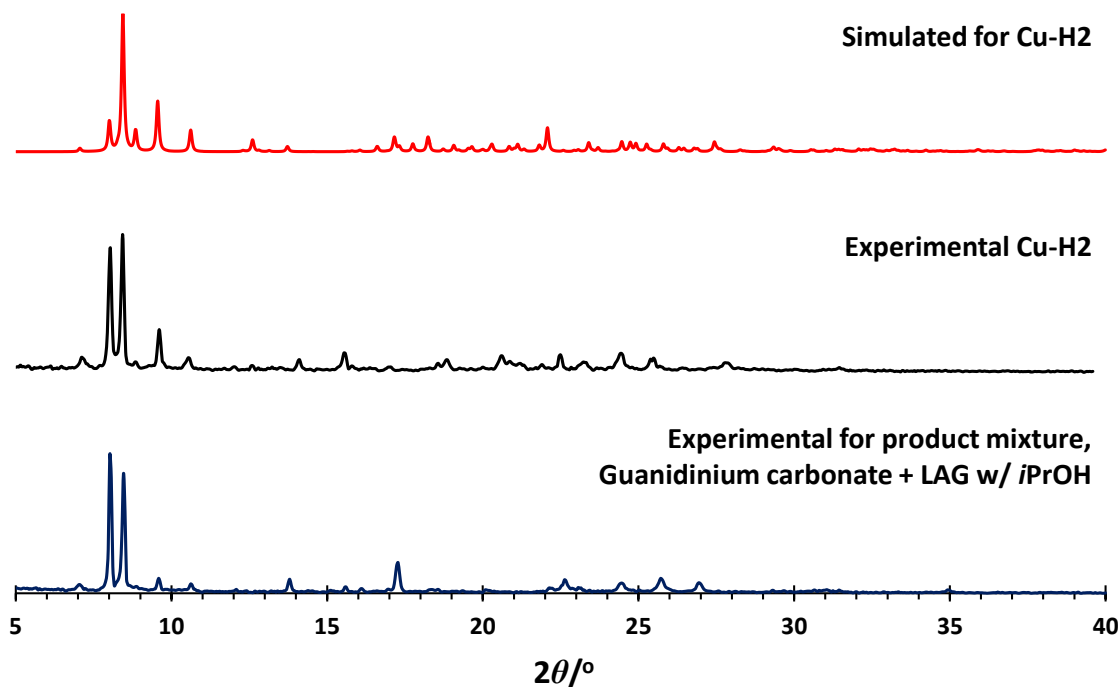


Figure S22. Simulated and experimentally acquired PXRD pattern of **Cu-H2** using Cu(OTf)₂.

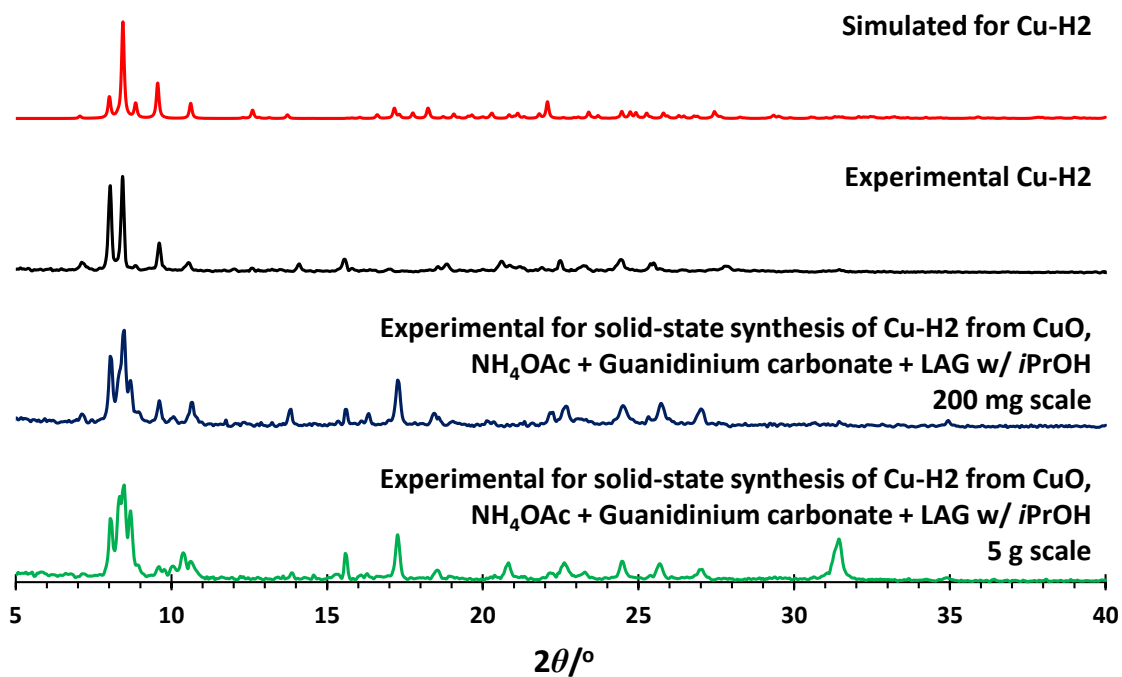


Figure S23. Simulated and experimentally acquired PXRD pattern of **Cu-H2** using CuO.

6. HR-MS Spectra

Mass Spectrum SmartFormula Report

Analysis Info

Analysis Name D:\Data\Friscic\2020-08-18 Friscic-Do JLD-H-Ligand ESI +ve.d
Method Tune_neg_Low_Na_Formate_100-1000.m
Sample Name 2020-08-18 Friscic-Do JLD-H-Ligand ESI +ve
Comment

Acquisition Date 8/18/2020 2:43:47 PM
Operator Alex
Instrument maXis impact 282001.00044

Acquisition Parameter

Source Type	ESI	Ion Polarity	Negative	Set Nebulizer	1.0 Bar
Focus	Not active	Set Capillary	4500 V	Set Dry Heater	180 °C
Scan Begin	100 m/z	Set End Plate Offset	-500 V	Set Dry Gas	4.0 l/min
Scan End	1000 m/z	Set Charging Voltage	2000 V	Set Divert Valve	Source
		Set Corona	0 nA	Set APCI Heater	0 °C

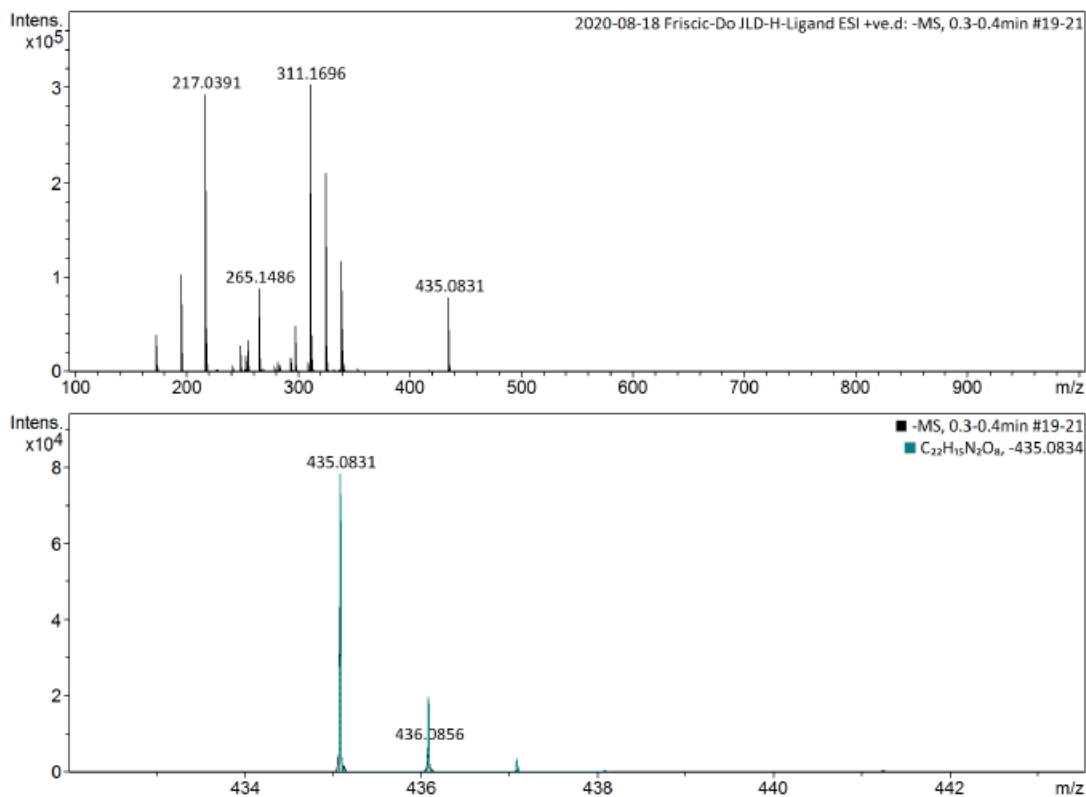


Figure S24. HR-MS spectrum for H₄L.

Mass Spectrum SmartFormula Report

Analysis Info

Analysis Name D:\Data\Friscic\2020-07-16 Friscic-Do JLD-Fe-H1-Na ESI -ve.d Acquisition Date 7/16/2020 11:45:39 AM
Method Tune_neg_Mid_AW.m Operator Alex
Sample Name 2020-07-16 Friscic-Do JLD-Fe-H1-Na ESI -ve Instrument maXis impact 282001.00044
Comment

Acquisition Parameter

Source Type	ESI	Ion Polarity	Negative	Set Nebulizer	0.4 Bar
Focus	Not active	Set Capillary	3500 V	Set Dry Heater	180 °C
Scan Begin	50 m/z	Set End Plate Offset	-500 V	Set Dry Gas	4.0 l/min
Scan End	3000 m/z	Set Charging Voltage	2000 V	Set Divert Valve	Source
		Set Corona	0 nA	Set APCI Heater	0 °C

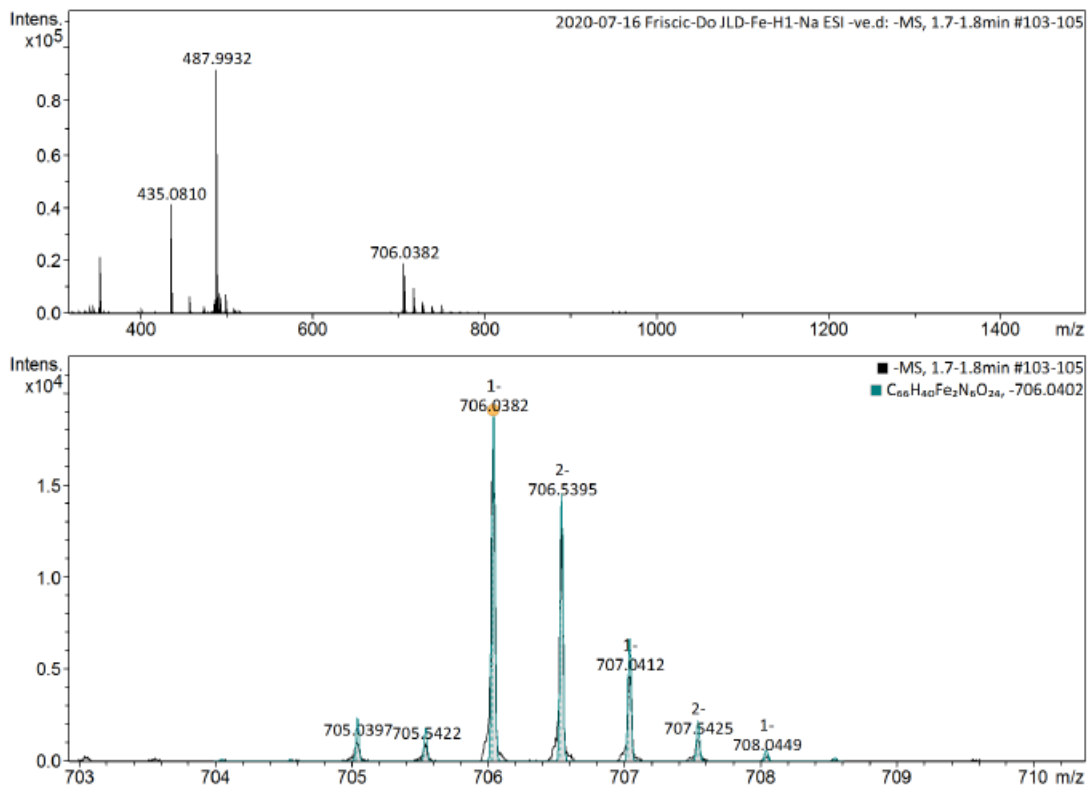


Figure S25. HR-MS spectrum for Fe-H1 made in solution.

Mass Spectrum SmartFormula Report

Analysis Info

Analysis Name D:\Data\Friscic\2020-07-16 Friscic-Do JLD-Fe-H2-Na-But ESI -ve.d
Method Tune_neg_Mid_AW.m
Sample Name 2020-07-16 Friscic-Do JLD-Fe-H2-Na-But ESI -ve
Comment

Acquisition Date 7/16/2020 12:12:42 PM

Operator Alex
Instrument maXis impact 282001.00044

Acquisition Parameter

Source Type	ESI	Ion Polarity	Negative	Set Nebulizer	0.4 Bar
Focus	Not active	Set Capillary	3500 V	Set Dry Heater	180 °C
Scan Begin	50 m/z	Set End Plate Offset	-500 V	Set Dry Gas	4.0 l/min
Scan End	3000 m/z	Set Charging Voltage	2000 V	Set Divert Valve	Source
		Set Corona	0 nA	Set APCI Heater	0 °C

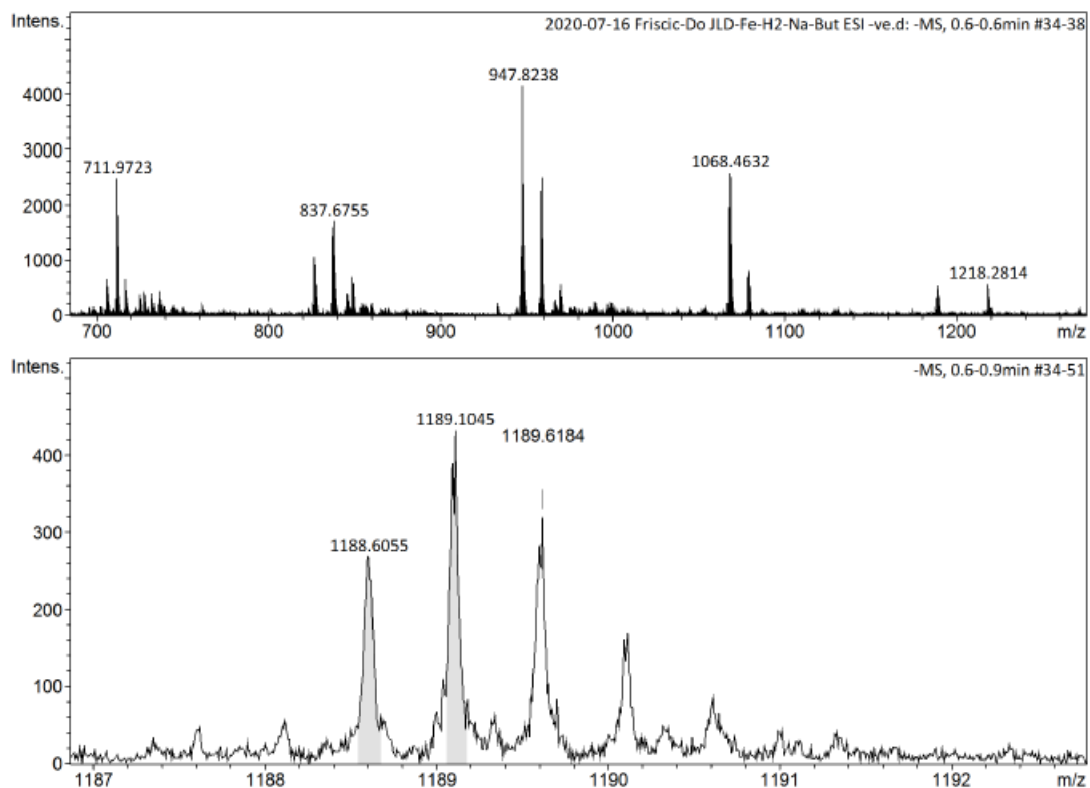


Figure S26. HR-MS spectrum for Fe-H2 made in solution.

Mass Spectrum SmartFormula Report

Analysis Info

Analysis Name D:\Data\Friscic\2020-07-16 Friscic-Do JLD-Fe-H3-TMEDA ESI -ve.d Acquisition Date 7/16/2020 12:44:13 PM
Method Tune_neg_Mid_AW.m Operator Alex
Sample Name 2020-07-16 Friscic-Do JLD-Fe-H3-TMEDA ESI -ve Instrument maXis impact 282001.0004
Comment

Acquisition Parameter

Source Type	ESI	Ion Polarity	Negative	Set Nebulizer	0.4 Bar
Focus	Not active	Set Capillary	3500 V	Set Dry Heater	180 °C
Scan Begin	50 m/z	Set End Plate Offset	-500 V	Set Dry Gas	4.0 l/min
Scan End	3000 m/z	Set Charging Voltage	2000 V	Set Divert Valve	Source
		Set Corona	0 nA	Set APCI Heater	0 °C

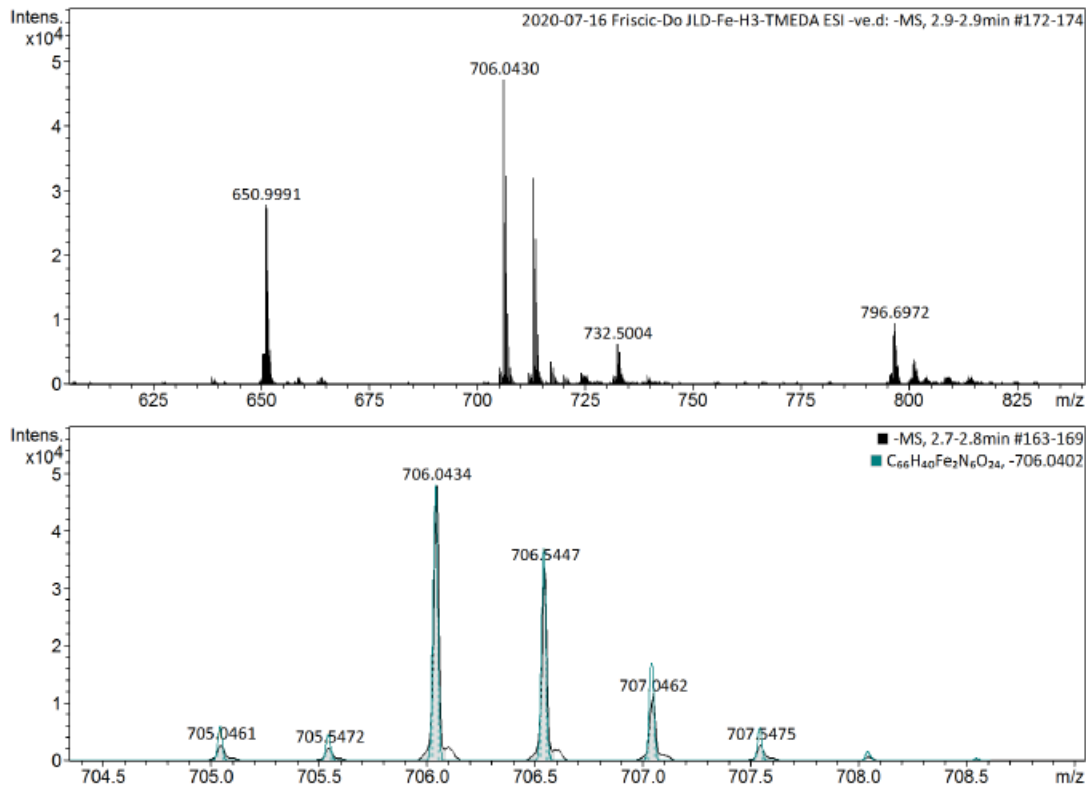


Figure S27. HR-MS spectrum for Fe-H3 made in solution.

Display Report

Analysis Info

Analysis Name D:\Data\Friscic\2020-07-16 Friscic-Do JLD-Fe-H4-Gua ESI -ve.d
Method Tune_neg_Mid_AW.m
Sample Name 2020-07-16 Friscic-Do JLD-Fe-H4-Gua ESI -ve
Comment

Acquisition Date 7/16/2020 1:49:23 PM

Operator Alex
Instrument maXis impact 282001.00044

Acquisition Parameter

Source Type	ESI	Ion Polarity	Negative	Set Nebulizer	0.4 Bar
Focus	Not active	Set Capillary	3500 V	Set Dry Heater	180 °C
Scan Begin	50 m/z	Set End Plate Offset	-500 V	Set Dry Gas	4.0 l/min
Scan End	3000 m/z	Set Charging Voltage	2000 V	Set Divert Valve	Source
		Set Corona	0 nA	Set APCI Heater	0 °C

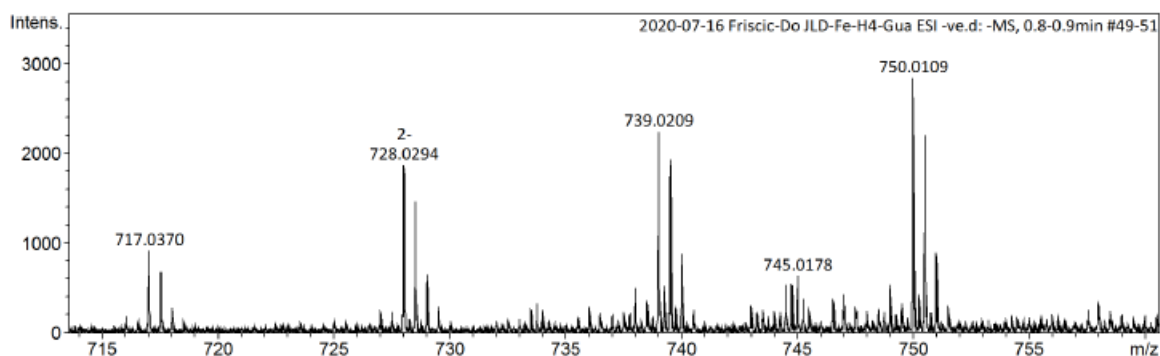
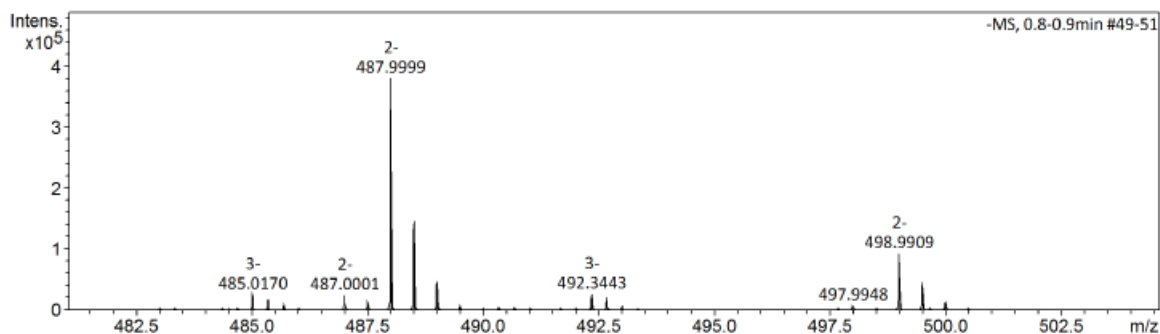
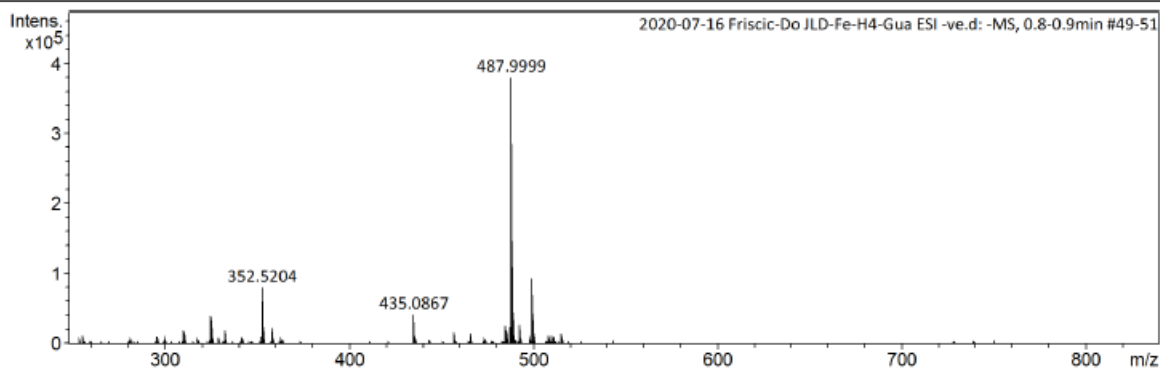


Figure S28. HR-MS spectrum for Fe-H4A made in solution.

Mass Spectrum SmartFormula Report

Analysis Info

Analysis Name D:\Data\Friscic\2020-07-16 Friscic-Do JLD-Cu-H1-Na ESI -ve.d
Method Tune_neg_Mid_AW.m
Sample Name 2020-07-16 Friscic-Do JLD-Cu-H1-Na ESI -ve
Comment

Acquisition Date 7/16/2020 1:28:56 PM
Operator Alex
Instrument maXis impact 282001.00044

Acquisition Parameter

Source Type	ESI	Ion Polarity	Negative	Set Nebulizer	0.4 Bar
Focus	Not active	Set Capillary	3500 V	Set Dry Heater	180 °C
Scan Begin	50 m/z	Set End Plate Offset	-500 V	Set Dry Gas	4.0 l/min
Scan End	3000 m/z	Set Charging Voltage	2000 V	Set Divert Valve	Source
		Set Corona	0 nA	Set APCI Heater	0 °C

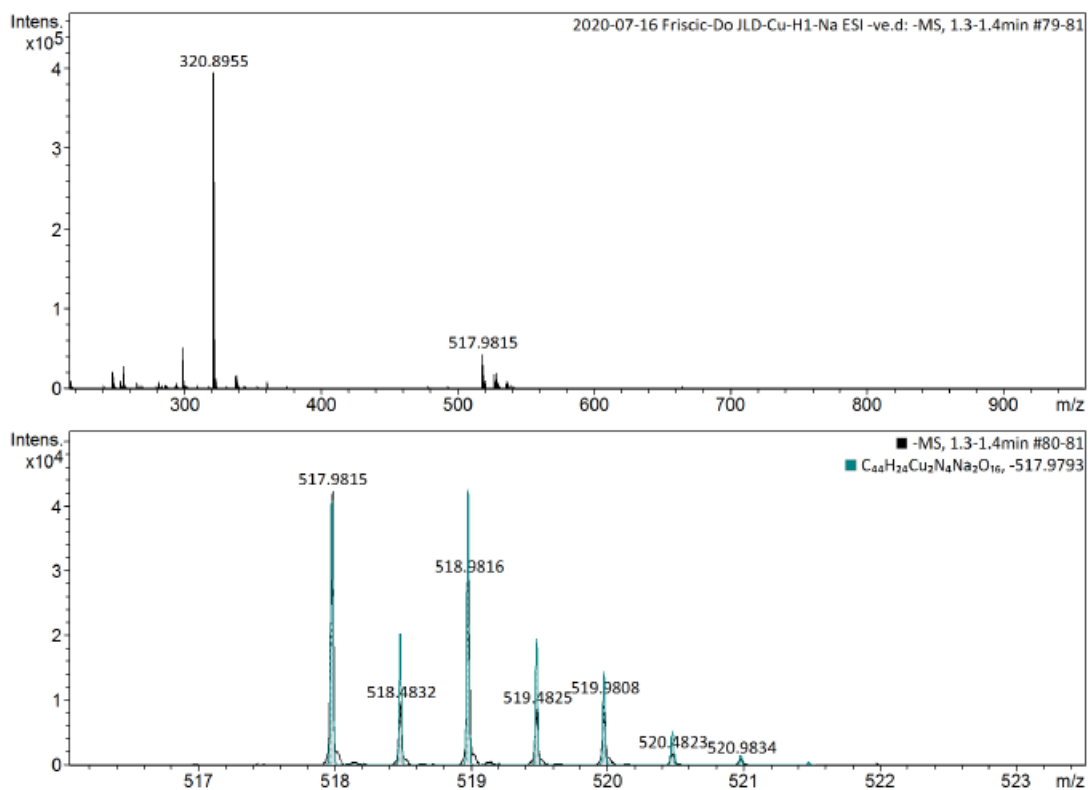


Figure S29. HR-MS spectrum for **Cu-H1** made in solution.

Mass Spectrum SmartFormula Report

Analysis Info

Analysis Name D:\Data\Friscic\2020-07-16 Friscic-Do JLD-Cu-H2-Gua ESI -ve.d Acquisition Date 7/16/2020 2:02:44 PM
Method Tune_neg_Mid_AW.m Operator Alex
Sample Name 2020-07-16 Friscic-Do JLD-Cu-H2-Gua ESI -ve Instrument maXis impact 282001.00044
Comment

Acquisition Parameter

Source Type	ESI	Ion Polarity	Negative	Set Nebulizer	0.4 Bar
Focus	Not active	Set Capillary	3500 V	Set Dry Heater	180 °C
Scan Begin	50 m/z	Set End Plate Offset	-500 V	Set Dry Gas	4.0 l/min
Scan End	3000 m/z	Set Charging Voltage	2000 V	Set Divert Valve	Source
		Set Corona	0 nA	Set APCI Heater	0 °C

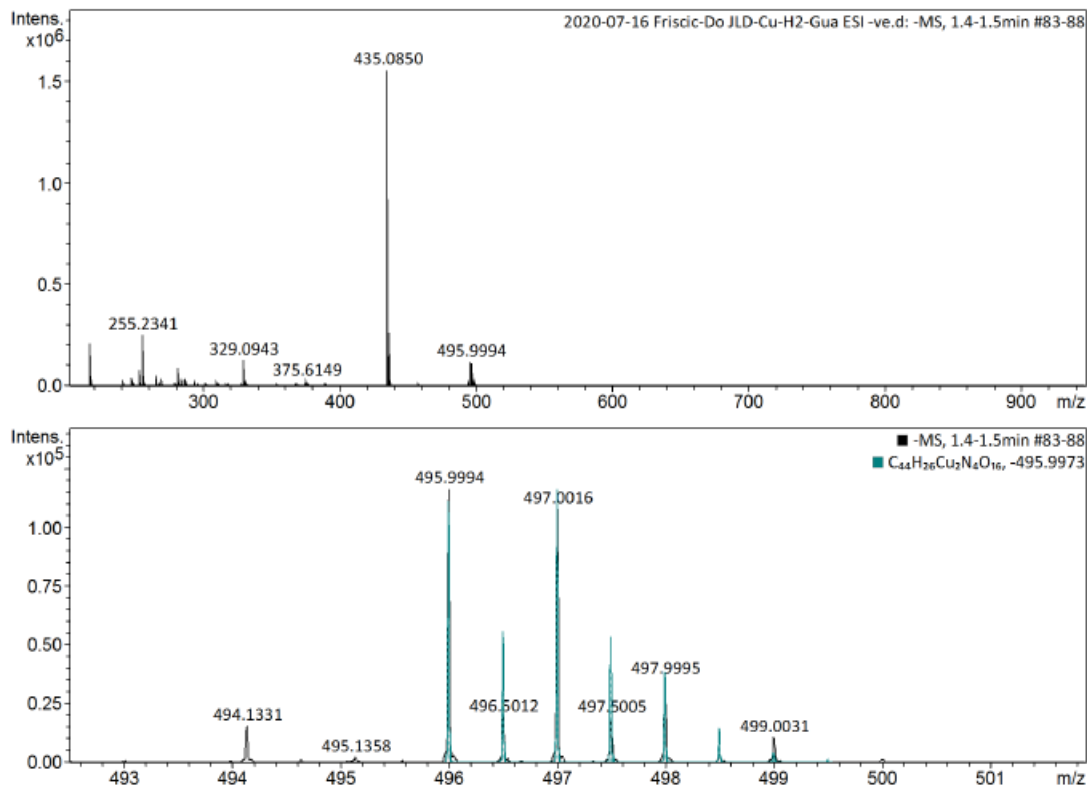


Figure S30. HR-MS spectrum for **Cu-H2** made in solution.

Mass Spectrum SmartFormula Report

Analysis Info

Analysis Name D:\Data\Friscic\2020-07-27 Friscic-Do JLD-Fe-H1-MC ESI -ve.d Acquisition Date 7/27/2020 4:49:30 PM
Method Tune_neg_Mid_AW.m Operator Alex
Sample Name 2020-07-27 Friscic-Do JLD-Fe-H1-MC ESI -ve Instrument maXis impact 282001.00044
Comment

Acquisition Parameter

Source Type	ESI	Ion Polarity	Negative	Set Nebulizer	0.4 Bar
Focus	Not active	Set Capillary	3500 V	Set Dry Heater	180 °C
Scan Begin	50 m/z	Set End Plate Offset	-500 V	Set Dry Gas	4.0 l/min
Scan End	3000 m/z	Set Charging Voltage	2000 V	Set Divert Valve	Source
		Set Corona	0 nA	Set APCI Heater	0 °C

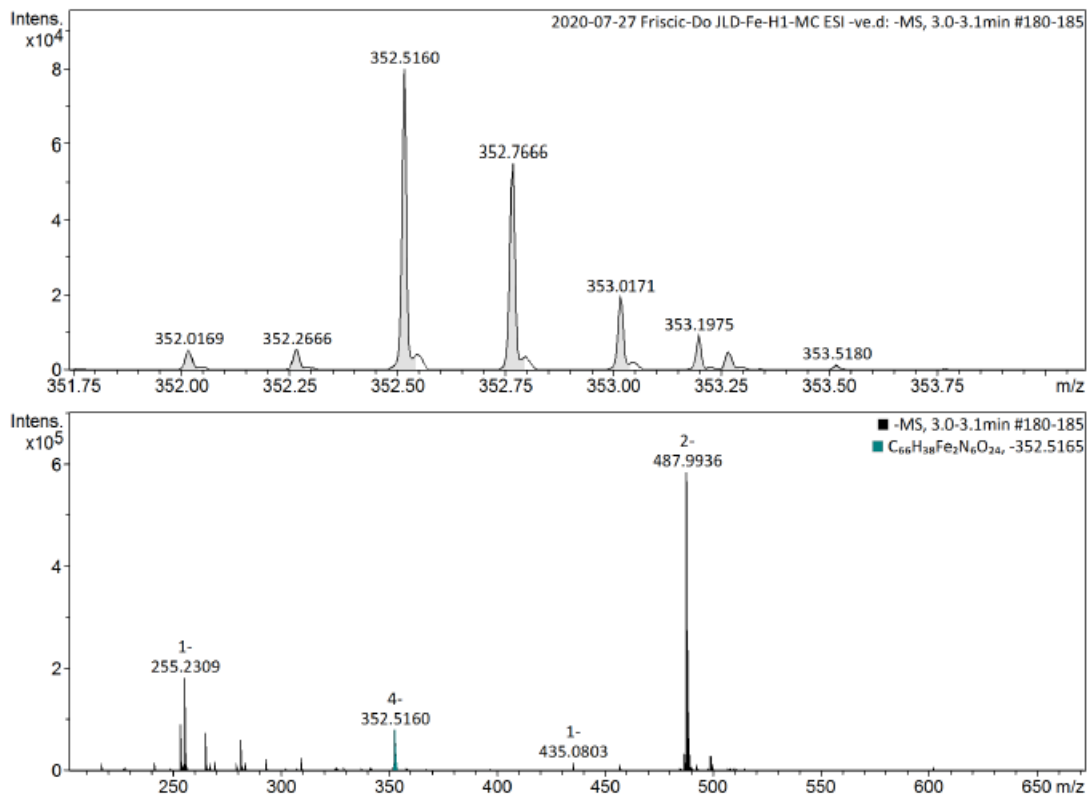


Figure S31. HR-MS spectrum for **Fe-H1** made mechanochemically.

Mass Spectrum SmartFormula Report

Analysis Info

Analysis Name D:\Data\Friscic\2020-07-27 Friscic-Do JLD-Fe-H2-MC ESI -ve.d
Method Tune_neg_Mid_AW.m
Sample Name 2020-07-27 Friscic-Do JLD-Fe-H2-MC ESI -ve
Comment

Acquisition Date 7/27/2020 5:17:48 PM
Operator Alex
Instrument maXis impact 282001.00044

Acquisition Parameter

Source Type	ESI	Ion Polarity	Negative	Set Nebulizer	0.4 Bar
Focus	Not active	Set Capillary	3500 V	Set Dry Heater	180 °C
Scan Begin	50 m/z	Set End Plate Offset	-500 V	Set Dry Gas	4.0 l/min
Scan End	3000 m/z	Set Charging Voltage	2000 V	Set Divert Valve	Source
		Set Corona	0 nA	Set APCI Heater	0 °C

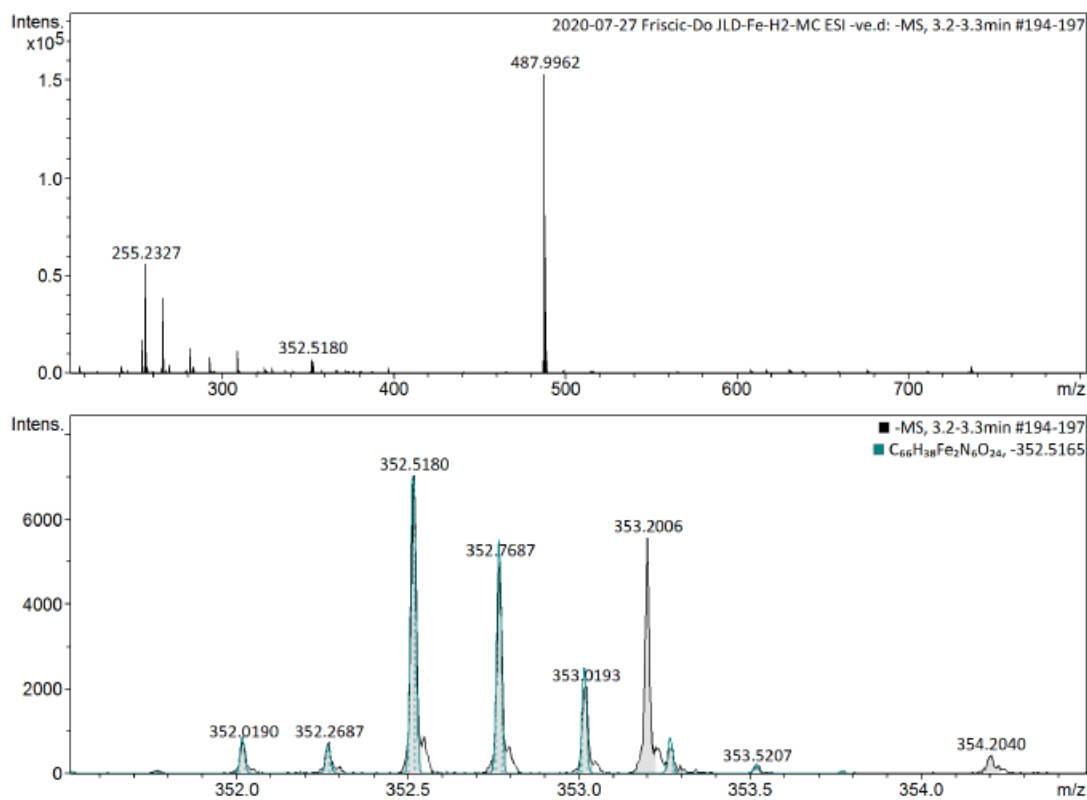


Figure S32. HR-MS spectrum for Fe-H2 made mechanochemically.

Mass Spectrum SmartFormula Report

Analysis Info

Analysis Name D:\Data\Friscic\2020-07-27 Friscic-Do JLD-Fe-H3-MC ESI -ve.d
Method Tune_neg_Mid_AW.m
Sample Name 2020-07-27 Friscic-Do JLD-Fe-H3-MC ESI -ve
Comment

Acquisition Date 7/27/2020 5:31:23 PM
Operator Alex
Instrument maXis impact 282001.00044

Acquisition Parameter

Source Type	ESI	Ion Polarity	Negative	Set Nebulizer	0.4 Bar
Focus	Not active	Set Capillary	3500 V	Set Dry Heater	180 °C
Scan Begin	50 m/z	Set End Plate Offset	-500 V	Set Dry Gas	4.0 l/min
Scan End	3000 m/z	Set Charging Voltage	2000 V	Set Divert Valve	Source
		Set Corona	0 nA	Set APCI Heater	0 °C

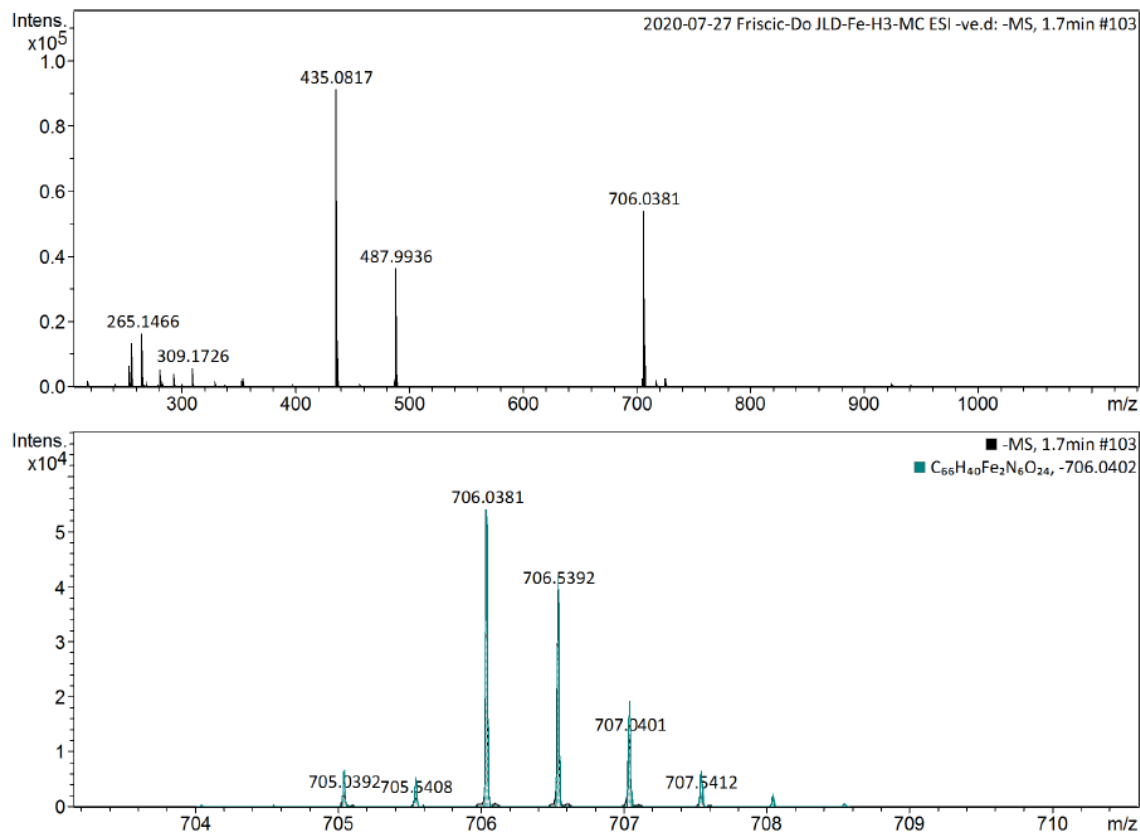


Figure S33. HR-MS spectrum for Fe-H3 made mechanochemically.

Mass Spectrum SmartFormula Report

Analysis Info

Analysis Name D:\Data\Friscic\2020-07-27 Friscic-Do JLD-Fe-H4-MC ESI -ve.d Acquisition Date 7/27/2020 6:01:11 PM
Method Tune_neg_Mid_AW.m Operator Alex
Sample Name 2020-07-27 Friscic-Do JLD-Fe-H4-MC ESI -ve Instrument maXis impact 282001.00044
Comment

Acquisition Parameter

Source Type	ESI	Ion Polarity	Negative	Set Nebulizer	0.4 Bar
Focus	Not active	Set Capillary	3500 V	Set Dry Heater	180 °C
Scan Begin	50 m/z	Set End Plate Offset	-500 V	Set Dry Gas	4.0 l/min
Scan End	3000 m/z	Set Charging Voltage	2000 V	Set Divert Valve	Source
		Set Corona	0 nA	Set APCI Heater	0 °C

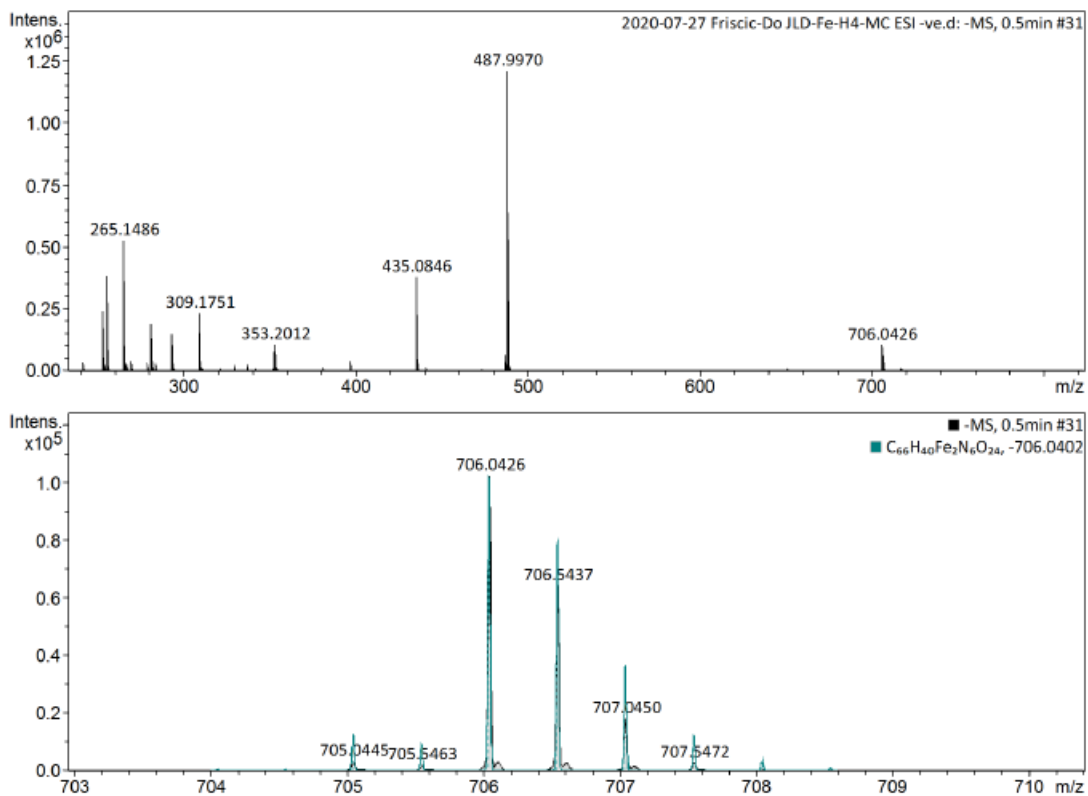


Figure S34. HR-MS spectrum for Fe-H4A made mechanochemically.

Mass Spectrum SmartFormula Report

Analysis Info

Analysis Name D:\Data\Friscic\2020-07-27 Friscic-Do JLD-Cu-H1-MC ESI -ve.d Acquisition Date 7/27/2020 6:14:23 PM
Method Tune_neg_Mid_AW.m Operator Alex
Sample Name 2020-07-27 Friscic-Do JLD-Cu-H1-MC ESI -ve Instrument maXis impact 282001.00044
Comment

Acquisition Parameter

Source Type	ESI	Ion Polarity	Negative	Set Nebulizer	0.4 Bar
Focus	Not active	Set Capillary	3500 V	Set Dry Heater	180 °C
Scan Begin	50 m/z	Set End Plate Offset	-500 V	Set Dry Gas	4.0 l/min
Scan End	3000 m/z	Set Charging Voltage	2000 V	Set Divert Valve	Source
		Set Corona	0 nA	Set APCI Heater	0 °C

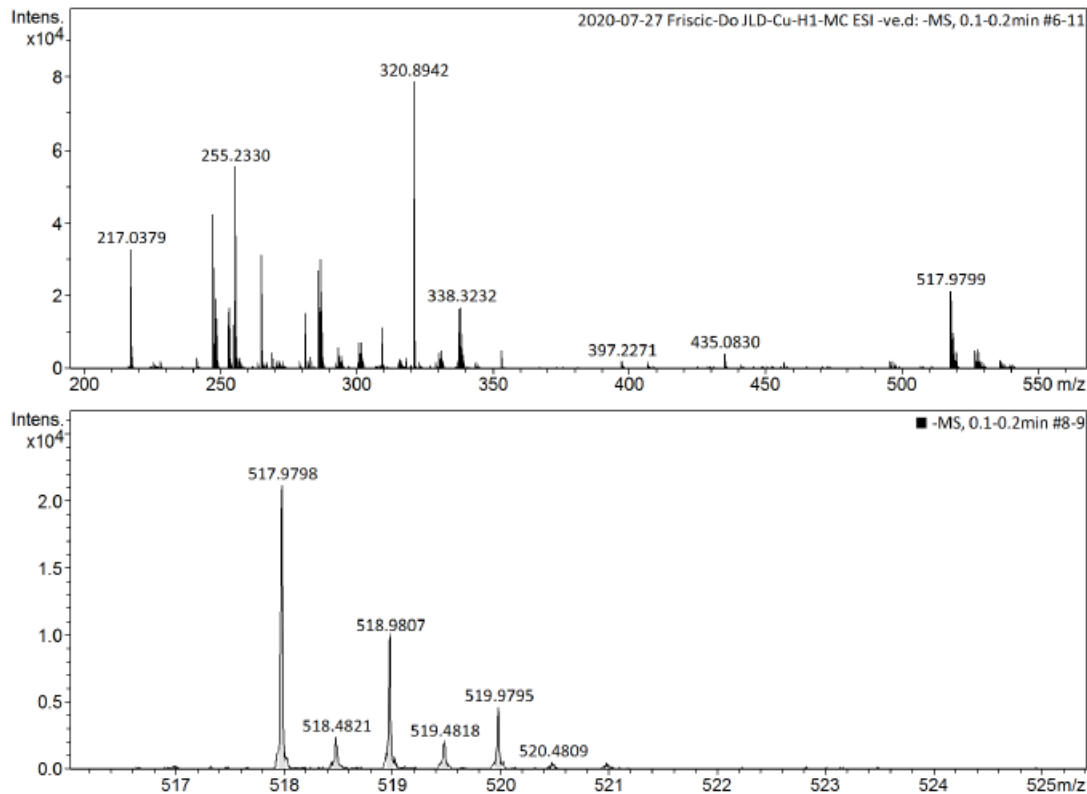


Figure S35. HR-MS spectrum for Cu-H1 made mechanochemically.

Mass Spectrum SmartFormula Report

Analysis Info

Analysis Name D:\Data\Friscic\2020-07-27 Friscic-Do JLD-Cu-H2-MC ESI -ve.d
Method Tune_neg_Mid_AW.m
Sample Name 2020-07-27 Friscic-Do JLD-Cu-H2-MC ESI -ve
Comment

Acquisition Date 7/27/2020 6:22:25 PM
Operator Alex
Instrument maXis impact 282001.00044

Acquisition Parameter

Source Type	ESI	Ion Polarity	Negative	Set Nebulizer	0.4 Bar
Focus	Not active	Set Capillary	3500 V	Set Dry Heater	180 °C
Scan Begin	50 m/z	Set End Plate Offset	-500 V	Set Dry Gas	4.0 l/min
Scan End	3000 m/z	Set Charging Voltage	2000 V	Set Divert Valve	Source
		Set Corona	0 nA	Set APCI Heater	0 °C

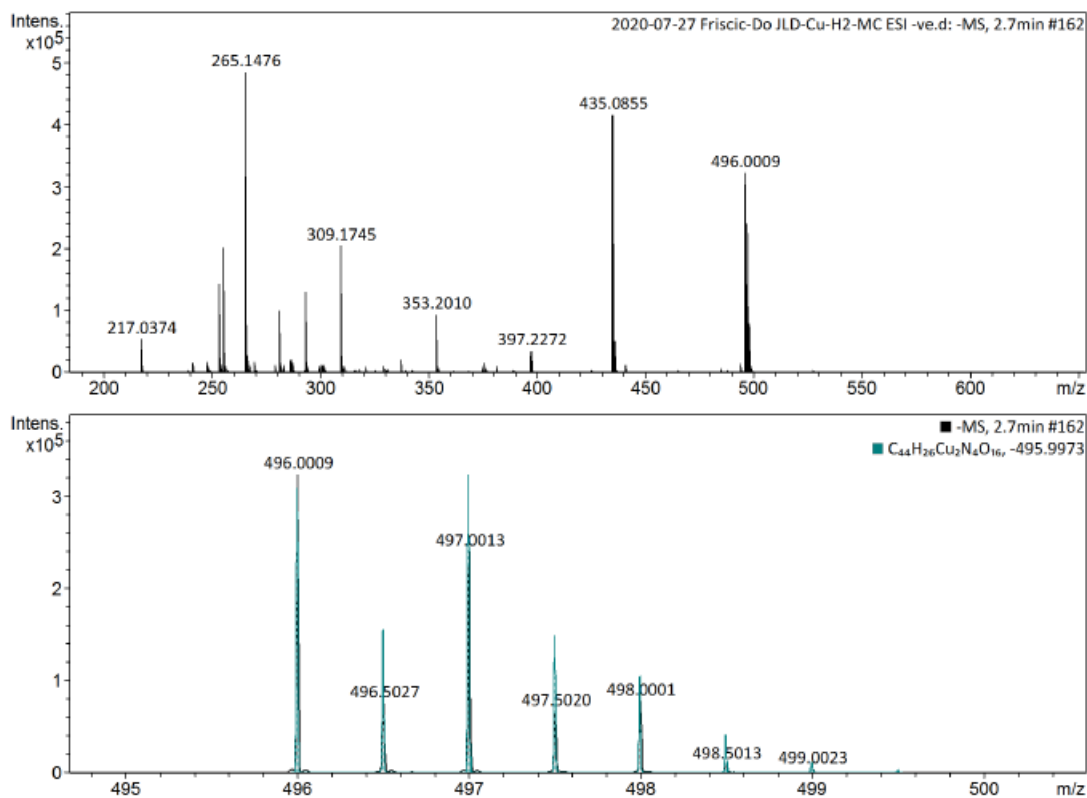


Figure S36. HR-MS spectrum for **Cu-H2** made mechanochemically from Cu(OTf)₂.

Mass Spectrum SmartFormula Report

Analysis Info

Analysis Name D:\Data\Friscic\2020-07-27 Friscic-Do JLD-Cu-H2-O ESI -ve.d
Method Tune_neg_Mid_AW.m
Sample Name 2020-07-27 Friscic-Do JLD-Cu-H2-O ESI -ve
Comment

Acquisition Date 7/27/2020 6:44:25 PM
Operator Alex
Instrument maXis impact 282001.00044

Acquisition Parameter

Source Type	ESI	Ion Polarity	Negative	Set Nebulizer	0.4 Bar
Focus	Not active	Set Capillary	3500 V	Set Dry Heater	180 °C
Scan Begin	50 m/z	Set End Plate Offset	-500 V	Set Dry Gas	4.0 l/min
Scan End	3000 m/z	Set Charging Voltage	2000 V	Set Divert Valve	Source
		Set Corona	0 nA	Set APCI Heater	0 °C

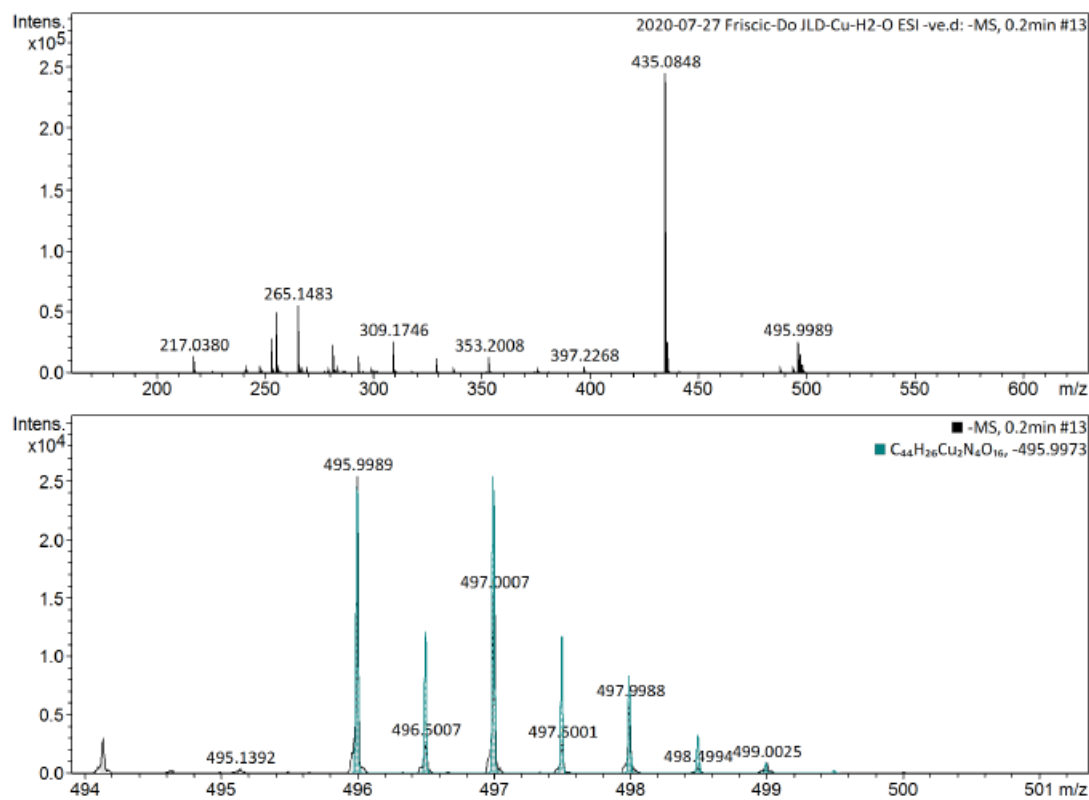


Figure S37. HR-MS spectrum for **Cu-H2** made mechanochemically from CuO.

7. Single Crystal X-ray Diffraction Data

Single crystal X-ray diffraction (SCXRD) data were measured on a Bruker D8 Venture diffractometer equipped with a Photon 200 area detector, and I μ S microfocus X-ray source (Bruker AXS, CuK α source). Crystals of **Fe-H1** were isolated on glass slides precooled using dry ice. It should be noted, except for the case of **Fe-H4B**, that all crystals when isolated from the solution had to be placed immediately under a stream of cold nitrogen to avoid loss of solvent of crystallization. All measurements were carried out at 150(2)K, except **Fe-H4A** at 180(2)K and **Fe-H4B** at RT, on coated crystal samples with thin layer of amorphous paratone oil, which decreases the thermal motion effects, deterioration and structural disorder to improve the accuracy of the structural results. Structure solution was carried out using the SHELXTL package from Bruker.¹ The parameters were refined for all data by full-matrix-least-squares or F2 using SHELXL.² All structures exhibit low stability in both RT and low temperature and the contribution of disordered solvate and cation moieties that could not be reliably modeled by discrete atoms were subtracted by SQUEEZE procedure, using the PLATON software.³ For instance **Fe-H3** is twinned by inversion and also exhibits half cation, DMF and two water molecules, which were unsuccessfully resolved. Structures **Fe-H1**, **Fe-H2**, and **Cu-H1** contain disordered water molecules, while **Cu-H2** contains disordered half *i*PrOH. All of the non-hydrogen atoms were refined with anisotropic thermal parameters. Hydrogen atoms were placed in calculated positions and allowed to ride on the carrier atoms. All hydrogen atom thermal parameters were constrained to ride on the carrier atom.

Table S1. Crystal data for the prepared Fe(III) and Cu(II) helicate solids.

	Fe-H1	Fe-H2	Fe-H3	Fe-H4A	Fe-H4B	Cu-H1	Cu-H2
Empirical formula	$C_{90}H_{97}Fe_2N_{11}Na_6O_{36}$	$C_{266}H_{388}Fe_4N_{22}Na_4O_{57}$	$C_{84}H_{86}Fe_2N_{12}O_{26}$	$C_{144}H_{170}Fe_4N_{48}O_{61}$	$C_{144}H_{162}Fe_4N_{48}O_{57}$	$C_{53}H_{47}Cu_2N_7Na_4O_{20}$	$C_{54}H_{65}Cu_2N_{16}O_{19}$
Formula weight/g mol ⁻¹	2158.42	5121.32	1791.34	3772.67	3700.61	1321.01	1369.30
Temperature/K	150(2)	150(2)	150(2)	180(2)	298(2)	150(2)	150(2)
Crystal system	monoclinic	monoclinic	orthorhombic	triclinic	monoclinic	monoclinic	monoclinic
Space group	<i>P</i> 2 ₁ / <i>c</i>	<i>P</i> 2 ₁ / <i>n</i>	<i>P</i> nn2	<i>P</i> -1	<i>C</i> 2/ <i>c</i>	<i>P</i> 2 ₁ / <i>n</i>	<i>C</i> 2/ <i>c</i>
<i>a</i> /Å	19.9223(9)	26.1720(7)	23.0817(5)	14.1272(12)	43.027(4)	13.5168(4)	26.6408(15)
<i>b</i> /Å	28.8141(14)	17.3890(5)	23.3506(5)	14.8356(14)	9.8262(8)	30.7906(11)	12.2924(7)
<i>c</i> /Å	17.4931(7)	31.5009(8)	10.0089(2)	20.7950(18)	20.9293(18)	14.0219(5)	22.7172(12)
α /°	90	90	90	89.584(4)	90	90	90
β /°	97.020(3)	95.918(2)	90	74.544(3)	107.536(4)	94.730(2)	110.066(2)
γ /°	90	90	90	77.368(4)	90	90	90
Volume/Å ³	9966.5(8)	14259.8(7)	5394.5(2)	4093.0(6)	8437.5(12)	5815.9(3)	6987.8(7)
<i>Z</i>	4	2	2	1	2	4	4
ρ_{calc} /cm ³	1.438	1.193	1.103	1.531	1.457	1.509	1.302
μ /mm ⁻¹	3.365	2.270	2.728	3.711	3.572	1.897	1.396
F(000)	4480.0	5484.0	1868.0	1972.0	3844.0	2704.0	2844.0
2 θ range for data collection/°	4.468 to 144.76	4.632 to 145.138	5.384 to 144.794	6.114 to 144.71	8.608 to 144.53	6.946 to 145.632	8.856 to 146.156
Reflections collected	183477	1518319	81953	125279	42656	56134	55069
Independent reflections	19672 [R _{int} = 0.1499, R _{sigma} = 0.0842]	28059 [R _{int} = 0.1092, R _{sigma} = 0.0725]	10327 [R _{int} = 0.0962, R _{sigma} = 0.0637]	16141 [R _{int} = 0.1771, R _{sigma} = 0.0908]	8023 [R _{int} = 0.0951, R _{sigma} = 0.0664]	11419 [R _{int} = 0.0435, R _{sigma} = 0.0358]	6868 [R _{int} = 0.0438, R _{sigma} = 0.0247]
Data/restraints/parameters	19672/1620/1348	28059/2857/1779	10327/488/566	16141/1056/11214	8023/571/659	11416/921/777	6868/9/416
Goodness-of-fit on F ²	1.051	1.056	1.012	1.014	1.076	1.073	1.080
Final R indexes [I ≥ 2 σ (I)]	R ₁ = 0.1296, wR ₂ = 0.3298	R ₁ = 0.0905, wR ₂ = 0.2115	R ₁ = 0.0526, wR ₂ = 0.1399	R ₁ = 0.0804, wR ₂ = 0.1596	R ₁ = 0.0783, wR ₂ = 0.1909	R ₁ = 0.0705, wR ₂ = 0.2059	R ₁ = 0.0435, wR ₂ = 0.1078
Final R indexes [all data]	R ₁ = 0.1577, wR ₂ = 0.3502	R ₁ = 0.1264, wR ₂ = 0.2296	R ₁ = 0.0797, wR ₂ = 0.1593	R ₁ = 0.1383, wR ₂ = 0.1952	R ₁ = 0.0992, wR ₂ = 0.2041	R ₁ = 0.0841, wR ₂ = 0.22202	R ₁ = 0.0464, wR ₂ = 0.1098
Largest diff. peak/hole / e Å ⁻³	1.29/-2.20	1.50/-0.92	0.25/-0.28	1.03/-1.15	0.60/-0.65	0.97/-1.17	0.30/-0.42

Table S2. Hydrogen Bonds for Fe-H1

D	H	A	d(D-H)/Å	d(H-A)/Å	d(D-A)/Å	D-H-A/°
C1V	H1V	O18A	0.95	2.63	3.35(2)	133.6
O1	H1B	O31B ¹	0.84	2.46	3.064(7)	129.5
O2S	H2SA	O18B ²	0.82	2.52	3.099(10)	128.6
O2S	H2SA	O19B ²	0.82	2.43	3.250(10)	178.6
O2S	H2SB	O17A	0.90	2.33	2.881(9)	119.6
O2S	H2SB	O30C	0.90	2.50	3.394(10)	171.7
C11A	H11A	O8A	0.95	2.42	2.970(12)	116.9
C24A	H24A	O21A	0.95	2.33	2.902(11)	118.0
N9B	H9B	O16B	0.88	2.10	2.535(8)	110.0
C11B	H11B	O8B	0.95	2.35	2.911(12)	117.2
C11B	H11B	O1K	0.95	2.58	3.49(3)	159.7
C24B	H24B	O21B	0.95	2.40	2.922(10)	114.3
C11C	H11C	O8C	0.95	2.32	2.896(11)	118.6
C24C	H24C	O21C	0.95	2.27	2.881(10)	120.9
C2D	H2D	O32A	0.95	2.47	3.192(9)	133.0
C5D	H5DC	O29A ³	0.98	2.50	3.367(11)	147.9
C2F	H2F	O31B ¹	0.95	2.39	3.161(9)	138.0
C5F	H5FC	O29B ⁴	0.98	2.59	3.500(10)	155.4
O1T	H1TA	O19C ²	0.92	2.14	3.061(14)	175.7
O2T	H2TA	O1R	0.78	2.23	2.925(12)	149.7
O2T	H2TB	O21B ³	0.89	2.01	2.908(9)	178.8
C4V	H4VA	O8C ⁵	0.98	2.46	3.37(2)	154.1
C4V	H4VC	O21B ⁶	0.98	2.39	3.34(2)	163.1
C4L	H4LB	O1T ⁷	0.98	2.61	3.48(3)	147.3
C3L	H3LA	O1I ⁸	0.98	2.39	3.37(5)	174.4
C3L	H3LB	O2S ⁷	0.98	2.39	3.29(4)	152.3
C5U	H5U1	O21C ⁸	0.98	2.09	3.02(10)	157.4
C5I	H5I1	O1I	0.98	2.01	2.52(3)	110.3
C5I	H5I2	O21C ⁸	0.98	2.32	3.28(3)	166.2

Symmetry codes: (1) 1+X,+Y,+Z;(2) -1+X,+Y,+Z; (3)+X,1/2-Y,1/2+Z; (4) 1+X,1/2-Y,-1/2+Z; (5) 1-X,1-Y,-Z; (6) 1-X,1/2+Y,1/2-Z; (7) 1-X,1-Y,1-Z; (8) 2-X,1-Y,1-Z

Table S3. Hydrogen Bonds for Fe-H2.

D	H	A	d(D-H)/Å	d(H-A)/Å	d(D-A)/Å	D-H-A/°
O12	H04R	O31C ¹	0.87	1.88	2.722(5)	161.4
N9A	H9A	O16A	0.88	2.14	2.578(4)	110.2
C11A	H11A	O8A	0.95	2.32	2.905(6)	119.0
N22A	H22A	O29A	0.88	2.11	2.550(4)	110.5
C24A	H24A	O21A	0.95	2.33	2.915(6)	119.4
N9B	H9B	O16B	0.78(5)	2.11(5)	2.530(4)	114(4)
C11B	H11B	O8B	0.95	2.45	3.006(5)	117.0
C24B	H24B	O21B	0.95	2.32	2.907(6)	119.5
C11C	H11C	O8C	0.95	2.30	2.896(5)	120.2
C24C	H24C	O21C	0.95	2.24	2.849(6)	120.8
C7D	H7DB	O18A	0.99	2.30	3.196(9)	150.6
C10D	H10A	O18C ²	0.99	2.53	3.523(6)	178.3
C2E	H2EA	O8C ³	0.99	2.45	3.335(6)	148.8
C2E	H2EB	O8B ³	0.99	2.41	3.274(6)	146.0
C10E	H10C	O32B	0.99	2.51	3.392(6)	148.7
C10E	H10D	O18B ¹	0.99	2.64	3.533(6)	149.7
C14E	H14C	O8B ³	0.99	2.45	3.328(5)	147.0
C14E	H14D	O8C ³	0.99	2.48	3.347(6)	145.9
C6F	H6F1	O4T	0.99	2.34	3.313(8)	169.2
C6F	H6F2	O31C ¹	0.99	2.59	3.510(9)	154.3
C11F	H11H	O32B	0.99	2.49	3.298(7)	138.1
O5T	H1A	O18B	0.94	1.92	2.817(4)	158.2
O5T	H1A	O19B	0.94	2.65	3.119(4)	111.1
O5T	H1	O18C ²	0.94	1.79	2.704(4)	162.5
O5T	H1	O19C ²	0.94	2.47	3.165(4)	130.2
O4T	H4TB	O32B	0.92	1.88	2.745(5)	155.6
C5P	H5PA	O21A	0.99	2.52	3.328(15)	139.0
C5P	H5PB	O21C	0.99	2.34	3.248(14)	152.5
C10P	H10G	O21C	0.99	2.26	3.22(4)	164.2
C13P	H13M	O21C	0.99	2.62	3.491(13)	146.3
C13P	H13N	O21A	0.99	2.57	3.318(15)	132.4
C14P	H14G	O31C ⁴	0.99	2.55	3.420(14)	145.9
C1G	H1GA	O21A	0.99	2.50	3.349(18)	144.0
C1G	H1GB	O21C	0.99	2.49	3.325(17)	141.9

C2G	H2GA	O31C ⁴	0.99	2.46	3.44(2)	169.6
C5G	H5GA	O32C ⁴	0.99	2.53	3.37(2)	142.0
C9G	H9GA	O21A	0.99	2.33	3.150(19)	139.6
C9G	H9GB	O21C	0.99	2.45	3.34(2)	149.3
C13G	H13P	O3T ⁴	0.99	2.51	3.17(2)	124.1

Symmetry codes: (1) 1/2+X,3/2-Y,-1/2+Z; (2) -1/2+X,3/2-Y,1/2+Z; (3) 3/2-X,-1/2+Y,1/2-Z; (4) 1/2-X,1/2+Y,1/2-Z

Table 6 Hydrogen Bonds for r3.

D	H	A	d(D-H)/Å	d(H-A)/Å	d(D-A)/Å	D-H-A/°
O12	H04R	O31C ¹	0.87	1.88	2.722(5)	161.4
N9A	H9A	O16A	0.88	2.14	2.578(4)	110.2
C11A	H11A	O8A	0.95	2.32	2.905(6)	119.0
N22A	H22A	O29A	0.88	2.11	2.550(4)	110.5
C24A	H24A	O21A	0.95	2.33	2.915(6)	119.4
N9B	H9B	O16B	0.78(5)	2.11(5)	2.530(4)	114(4)
C11B	H11B	O8B	0.95	2.45	3.006(5)	117.0
C24B	H24B	O21B	0.95	2.32	2.907(6)	119.5
C11C	H11C	O8C	0.95	2.30	2.896(5)	120.2
C24C	H24C	O21C	0.95	2.24	2.849(6)	120.8
C7D	H7DB	O18A	0.99	2.30	3.196(9)	150.6
C10D	H10A	O18C ²	0.99	2.53	3.523(6)	178.3
C2E	H2EA	O8C ³	0.99	2.45	3.335(6)	148.8
C2E	H2EB	O8B ³	0.99	2.41	3.274(6)	146.0
C10E	H10C	O32B	0.99	2.51	3.392(6)	148.7
C10E	H10D	O18B ¹	0.99	2.64	3.533(6)	149.7
C14E	H14C	O8B ³	0.99	2.45	3.328(5)	147.0
C14E	H14D	O8C ³	0.99	2.48	3.347(6)	145.9
C6F	H6F1	O4T	0.99	2.34	3.313(8)	169.2
C6F	H6F2	O31C ¹	0.99	2.59	3.510(9)	154.3
C11F	H11H	O32B	0.99	2.49	3.298(7)	138.1
O5T	H1A	O18B	0.94	1.92	2.817(4)	158.2
O5T	H1A	O19B	0.94	2.65	3.119(4)	111.1
O5T	H1	O18C ²	0.94	1.79	2.704(4)	162.5
O5T	H1	O19C ²	0.94	2.47	3.165(4)	130.2
O4T	H4TB	O32B	0.92	1.88	2.745(5)	155.6
C5P	H5PA	O21A	0.99	2.52	3.328(15)	139.0
C5P	H5PB	O21C	0.99	2.34	3.248(14)	152.5
C10P	H10G	O21C	0.99	2.26	3.22(4)	164.2
C13P	H13M	O21C	0.99	2.62	3.491(13)	146.3
C13P	H13N	O21A	0.99	2.57	3.318(15)	132.4
C14P	H14G	O31C ⁴	0.99	2.55	3.420(14)	145.9
C1G	H1GA	O21A	0.99	2.50	3.349(18)	144.0
C1G	H1GB	O21C	0.99	2.49	3.325(17)	141.9
C2G	H2GA	O31C ⁴	0.99	2.46	3.44(2)	169.6
C5G	H5GA	O32C ⁴	0.99	2.53	3.37(2)	142.0
C9G	H9GA	O21A	0.99	2.33	3.150(19)	139.6

C9G	H9GB	O21C	0.99	2.45	3.34(2)	149.3
C13G	H13P	O3T ⁴	0.99	2.51	3.17(2)	124.1

Table S4. Hydrogen Bonds for Fe-H3.

D	H	A	d(D-H)/Å	d(H-A)/Å	d(D-A)/Å	D-H-A/°
N7A	H7A	O13A	0.88	2.11	2.553(6)	110.7
N18	H18	O25	0.88	2.13	2.577(5)	111.1
N2B	H2B	O28 ¹	1.00	1.76	2.687(7)	151.7
N2B	H2B	O27 ¹	1.00	2.28	3.099(8)	138.7
N5B	H5B	O14A ²	1.00	2.28	3.000(6)	127.9
N5B	H5B	O16A ²	1.00	1.73	2.719(7)	167.7
C5A	H5A	O8A	0.95	2.36	2.938(8)	118.6
C20	H20	O17	0.95	2.34	2.930(9)	119.6
C7B	H7BC	O17 ³	0.98	2.54	3.458(12)	156.4
C6B	H6BC	O8A ³	0.98	2.49	3.161(11)	125.1
C1B	H1BC	O5D	0.98	2.53	3.370(18)	143.3
C4B	H4BA	O27 ¹	0.99	2.65	3.411(9)	133.8
C4B	H4BB	O5D	0.99	2.35	3.332(12)	169.8
C5	H5	O9	0.95	2.24	2.859(10)	122.0
C8B	H8B1	O17	0.98	2.52	3.500(12)	175.1
C8B	H8B2	O30 ⁴	0.98	2.64	3.622(14)	175.1

Symmetry codes: (1) 1/2-X,-1/2+Y,-1/2+Z; (2) -1/2+X,1/2-Y,-1/2+Z; (3) +X,+Y,-1+Z; (4) -1/2+X,1/2-Y,1/2+Z

Table S5. Hydrogen Bonds for Fe-H4A.

D	H	A	d(D-H)/Å	d(H-A)/Å	d(D-A)/Å	D-H-A/°
O2W	H2WA	O16C ¹	0.85	2.34	3.069(6)	144.4
O2W	H2WB	O3W	0.85	1.94	2.758(6)	161.8
O3W	H3WA	O29C ²	0.85	2.18	2.855(6)	136.7
O3W	H3WB	O19A ¹	0.85	2.16	2.908(6)	147.4
O6W	H6WA	O19A ³	0.85	1.99	2.806(6)	161.0
O6W	H6WB	O32B	0.85	1.95	2.795(6)	177.4
C11A	H11A	O8A	0.95	2.46	2.991(8)	115.5
C11A	H11A	N2E ⁴	0.95	2.68	3.416(8)	134.6
C24A	H24A	O21A	0.95	2.37	2.908(7)	115.8
N9B	H9B	O16B	0.88	2.04	2.505(6)	112.1
C15B	H15B	O8B	0.95	2.42	2.985(7)	117.5
C28B	H28B	O21B	0.95	2.40	2.929(7)	115.2
C15C	H15C	O8C	0.95	2.22	2.836(7)	121.4
O1W	H1WA	O19B ⁵	0.85	2.44	3.089(6)	133.2
O1W	H1WA	O32C ⁶	0.85	2.52	3.136(6)	130.5

O1W	H1WB	O19B	0.85	1.95	2.787(6)	169.3
C28C	H28C	O21C	0.95	2.26	2.866(7)	121.0
N2D	H2DA	O18C ⁷	0.88	2.55	3.323(6)	146.9
N2D	H2DA	O19C ⁷	0.88	2.25	3.054(7)	152.6
N2D	H2DB	O1W ⁷	0.88	2.50	3.206(7)	137.2
N3D	H3DA	O32B	0.88	2.04	2.904(7)	166.1
N3D	H3DB	O19C ⁷	0.88	2.41	3.182(7)	146.2
N4D	H4DA	O31B	0.88	2.04	2.920(6)	176.9
N4D	H4DB	O1W ⁷	0.88	2.55	3.245(7)	136.3
N4D	H4DB	O32C	0.88	2.42	3.152(7)	141.0
N2E	H2EA	O8B ¹	0.88	2.42	3.140(6)	139.1
N2E	H2EB	O8C	0.88	2.01	2.802(6)	149.5
N3E	H3EA	O8B ¹	0.88	2.01	2.833(6)	155.5
N3E	H3EB	O21A ⁸	0.88	2.04	2.867(6)	156.4
N4E	H4EA	O21A ⁸	0.88	2.38	3.117(6)	141.6
N4E	H4EB	O8C	0.88	2.16	2.915(6)	142.9
N4E	H4EB	O21C ⁴	0.88	2.32	2.800(6)	114.0
N2F	H2FA	O31A	0.81	2.24	3.020(7)	161.5
N2F	H2FB	O6W	0.81	2.22	2.896(7)	141.4
N3F	H3FA	O19B ³	0.88	2.11	2.982(6)	169.2
N3F	H3FB	O32A	0.88	2.14	2.948(7)	153.0
N4F	H4FA	O18B ³	0.88	2.30	3.026(6)	139.2
N4F	H4FB	N2BB	0.88	2.58	3.33(2)	143.9
N2G	H2GA	O2W	0.88	1.97	2.852(8)	174.3
N3G	H3GA	O1W ³	0.88	2.10	2.934(7)	158.4
N3G	H3GB	O3W	0.88	2.09	2.939(7)	162.1
N4G	H4GA	O1W ³	0.88	2.46	3.200(7)	142.5
N4G	H4GB	O32A	0.88	2.05	2.846(6)	149.7
N2H	H2HA	O18A ⁹	0.88	2.21	2.997(6)	148.2
N2H	H2HB	O7W ¹⁰	0.88	2.23	2.986(7)	144.1
N3H	H3HA	O18A ⁹	0.88	2.66	3.340(6)	135.2
N3H	H3HA	O19A ⁹	0.88	2.09	2.938(7)	162.9
N3H	H3HB	O19C	0.88	2.01	2.865(6)	163.1
N4H	H4HA	O7W ¹⁰	0.91	2.14	2.933(7)	145.1
N4H	H4HB	O18C	0.91	2.11	2.978(6)	159.0
N2AA	H2A2	O5W	0.88	1.90	2.769(13)	169.0
N3AA	H3AA	O31A ¹¹	0.88	2.58	3.280(10)	137.0
N3AA	H3AA	O31C ¹¹	0.88	2.12	2.925(9)	151.9
N3AA	H3AB	O4W	0.88	2.35	3.18(3)	157.9
N4AA	H4AB	O29A ¹¹	0.88	2.13	2.857(9)	139.8
N3BB	H3BA	O31A ¹¹	0.88	2.49	3.22(4)	141.2
N3BB	H3BA	O31C ¹¹	0.88	2.17	2.91(4)	141.9

N3BB	H3BB	O4X	0.88	1.90	2.74(8)	160.3
N4BB	H4BA	O29A ¹¹	0.88	2.38	3.14(3)	145.0
N4BB	H4BA	O31C ¹¹	0.88	2.46	3.15(3)	135.4
O7W	H7WA	O32A	0.91	2.08	2.872(6)	145.5
O7W	H7WB	O19C ¹	0.97	2.16	2.947(6)	136.7

Symmetry codes: (1) 1-X,1-Y,1-Z; (2) 1+X,+Y,+Z; (3) 1-X,2-Y,-Z; (4) 1+X,+Y,-1+Z; (5) -X,1-Y,1-Z; (6) -X,2-Y,2-Z; (7) +X,+Y,1+Z; (8) +X,+Y,-1+Z; (9) +X,-1+Y,+Z; (10) -X,1-Y,2-Z; (11) -1+X,+Y,1+Z

Table S6. Hydrogen Bonds for Fe-H4B.

D	H	A	d(D-H)/Å	d(H-A)/Å	d(D-A)/Å	D-H-A/°
O4W	H4WA	O2W	0.90	2.39	3.294(14)	179.1
O4W	H4WB	N4C ¹	0.90	2.42	3.114(13)	133.9
N9B	H9B	O21B ²	0.85(5)	2.05(5)	2.851(5)	156(5)
N22B	H22B	O1 ³	1.03	2.63	3.251(13)	118.5
N22B	H22B	O29B	1.03	2.07	2.623(4)	111.0
N22B	H22B	O2W ³	1.03	2.16	3.083(8)	147.7
O1	H1A	O8B	0.89	2.14	2.895(13)	142.4
O1	H1B	O29B ³	0.89	1.93	2.796(13)	163.9
O1	H1B	N3Z	0.89	2.46	2.95(3)	115.3
O1	H1B	N3Q	0.89	2.70	3.20(3)	116.7
C28B	H28B	O21B	0.93	2.46	2.920(6)	110.8
N6A	H6A	O1	0.87(5)	2.41(5)	3.183(14)	148(4)
C12A	H12A	O9V	0.93	2.56	3.04(3)	112.6
C12A	H12A	O10V ³	0.93	2.26	2.83(4)	118.9
N2Z	H2ZA	O1W ³	0.86	2.00	2.823(17)	158.8
N2Z	H2ZB	O2W ⁴	0.86	1.99	2.835(16)	168.0
O2W	H2WA	O8B	0.99	2.12	3.019(8)	149.9
O2W	H2WA	O1	0.99	2.57	3.336(16)	134.2
O2W	H2WB	O29B ³	1.00	2.14	3.097(7)	160.4
N3Z	H3Z1	O1W ³	0.86	2.56	3.24(2)	137.2
N3Z	H3Z2	O1	0.86	2.29	2.95(3)	134.6
N3Z	H3Z2	O29B ³	0.86	2.29	2.85(3)	123.1
N4Z	H4Z1	O13A	0.86	2.21	3.02(3)	157.8
N2C	H2CA	O4W	0.86	2.20	2.889(13)	136.7
N2C	H2CA	O16A ⁵	0.86	2.30	2.983(8)	136.2
N2C	H2CB	O19B ¹	0.86	1.85	2.685(8)	162.6
N3C	H3CA	O32B ⁶	0.86	2.14	2.945(10)	155.1
N3C	H3CB	O4W	0.86	2.26	2.946(13)	137.0
N4C	H4CA	O32B ⁶	0.86	2.41	3.141(8)	142.7
N4C	H4CB	O18B ¹	0.86	2.37	3.134(8)	148.2

N2D	H2DA	O31B ⁷	0.86	2.02	2.881(6)	176.0
N2D	H2DB	O16A ⁸	0.86	2.36	3.134(7)	150.5
N3D	H3DA	O32B ⁷	0.86	2.06	2.919(6)	172.2
N3D	H3DB	O16A	0.86	2.09	2.935(6)	169.7
N4D	H4DA	O15A	0.86	2.05	2.875(6)	161.7
O1W	H1WA	O21B	0.90	2.30	3.199(9)	179.6
O1W	H1WB	O9V	0.90	2.05	2.94(4)	172.8
O1W	H1WB	O10V ³	0.90	1.86	2.75(4)	173.0
N2Q	H2QA	O8B ⁴	0.86	2.20	2.929(18)	142.1
N2Q	H2QA	O2W ⁴	0.86	2.13	2.762(13)	129.6
N2Q	H2QB	O1W ³	0.86	2.27	3.046(15)	150.7
N3Q	H3Q1	O1	0.86	2.53	3.20(3)	134.9
N3Q	H3Q1	O29B ³	0.86	2.21	3.01(3)	153.3
N3Q	H3Q2	O1W ³	0.86	2.13	2.93(3)	154.7
N4Q	H4Q2	O13A	0.86	2.17	2.97(2)	154.8

Symmetry codes: (1) 1/2-X,1/2-Y,-Z; (2) 1-X,1-Y,1-Z; (3) 1-X,+Y,1/2-Z; (4) +X,1+Y,+Z; (5) +X,1-Y,-1/2+Z; (6) 1-X,-1+Y,1/2-Z; (7) -1/2+X,-1/2+Y,+Z; (8) 1/2-X,-1/2+Y,1/2-Z

Table S7. Hydrogen Bonds for Cu-H1.

D	H	A	d(D-H)/Å	d(H-A)/Å	d(D-A)/Å	D-H-A/°
N9B	H9B	O16B	0.88	2.07	2.521(4)	110.9
N22B	H22B	O29B	0.88	2.08	2.535(4)	111.0
N22A	H22A	O29A	0.88	2.08	2.539(5)	111.6
C11B	H11B	O8B	0.95	2.37	2.946(5)	118.6
C24A	H24A	O21A	0.95	2.40	2.968(6)	118.2
C24B	H24B	O21B	0.95	2.39	2.969(6)	119.1
C11A	H11A	O8A	0.95	2.40	2.970(5)	118.4
O1	H1B	O19B ¹	0.95	1.91	2.803(6)	154.7

Symmetry codes: (1) 1-X,1-Y,1-Z

Table S8. Hydrogen Bonds for Cu-H2.

D	H	A	d(D-H)/Å	d(H-A)/Å	d(D-A)/Å	D-H-A/°
N11	H11	O6	0.82(3)	2.15(3)	2.567(2)	112(2)
C28	H28	O21	0.95	2.38	2.904(3)	114.4
N2A	H2A1	O4 ¹	0.88	2.23	3.091(3)	164.6
N2A	H2A2	O21 ²	0.88	2.02	2.880(3)	165.7
N3A	H3A1	O13 ³	0.88	2.07	2.864(3)	149.5
N3A	H3A2	O3 ¹	0.88	2.14	2.999(3)	165.5
N4A	H4A1	O13 ³	0.88	2.19	2.951(3)	144.4
N4A	H4A2	O1W	0.88	2.02	2.894(4)	171.9
N2B	H2B1	O3 ³	0.88	2.27	3.024(3)	144.0
N2B	H2B2	O32	0.88	2.20	2.963(3)	144.7

N3B	H3B1	O31 ⁴	0.88	2.05	2.928(2)	174.7
N3B	H3B1	O32 ⁴	0.88	2.50	3.048(3)	120.8
N3B	H3B2	O3 ³	0.88	2.11	2.911(3)	150.3
N4B	H4B1	O3 ⁵	0.88	2.64	3.159(3)	119.0
N4B	H4B1	O4 ⁵	0.88	2.11	2.986(2)	171.1
N4B	H4B2	O32	0.88	2.06	2.863(3)	150.8
O4C	H4C	O6	0.89	1.94	2.834(3)	179.1
O1W	H1W	O21	0.90	1.95	2.854(3)	179.8

Symmetry codes: (1) 1-X,1-Y,-Z; ; (2) 1-X,+Y,1/2-Z; (3) 1-X,1+Y,1/2-Z; (4) 3/2-X,1/2+Y,3/2-Z; (5) 1/2+X,1/2+Y,1+Z

8. Thermogravimetric analysis

Table S9. Summary of Theoretical and Experimental Residues

Compound	Theoretical Residue (%)	Experimental Residue (%)
Fe-H1^a	22.1 (30.9) ^b	24.3 (29.2) ^c
Fe-H2	10.3	9.7
Fe-H3	8.3	7.7
Fe-H4A	8.4	8.6
Fe-H4B	8.7	9.2
Cu-H1	28.1	29.3
Cu-H2	11.6	11.3

^aMaterial rapidly loses solvent of crystallisation; ^bcalculated for material without any included solvent molecules; ^ccalculated by scaling the measured final residue (24.3%) by the approximate residue after desolvation (83.3%).

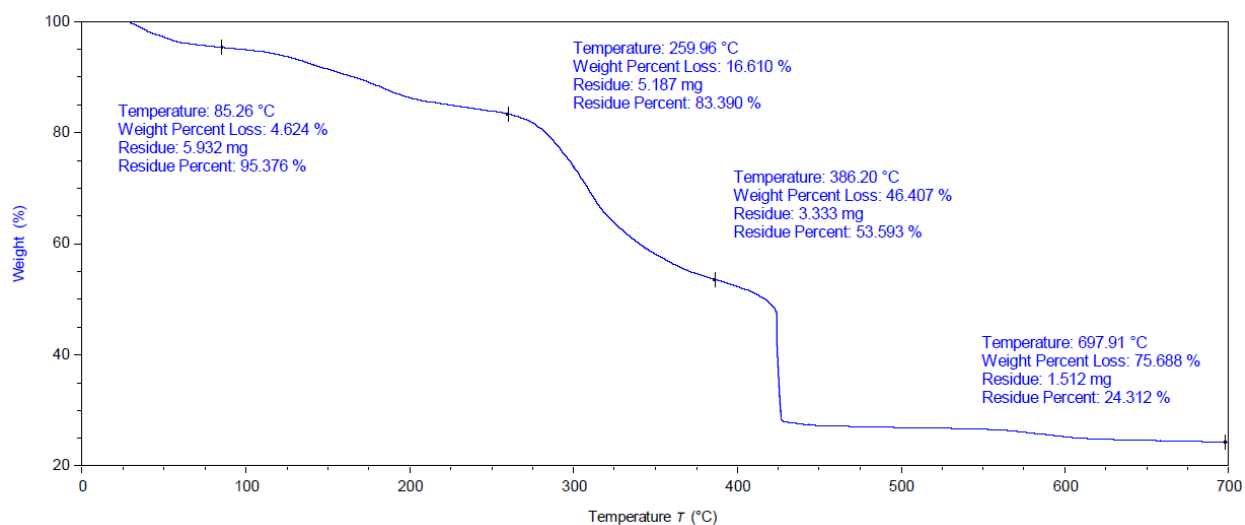


Figure S38. TGA thermogram of Fe-H1

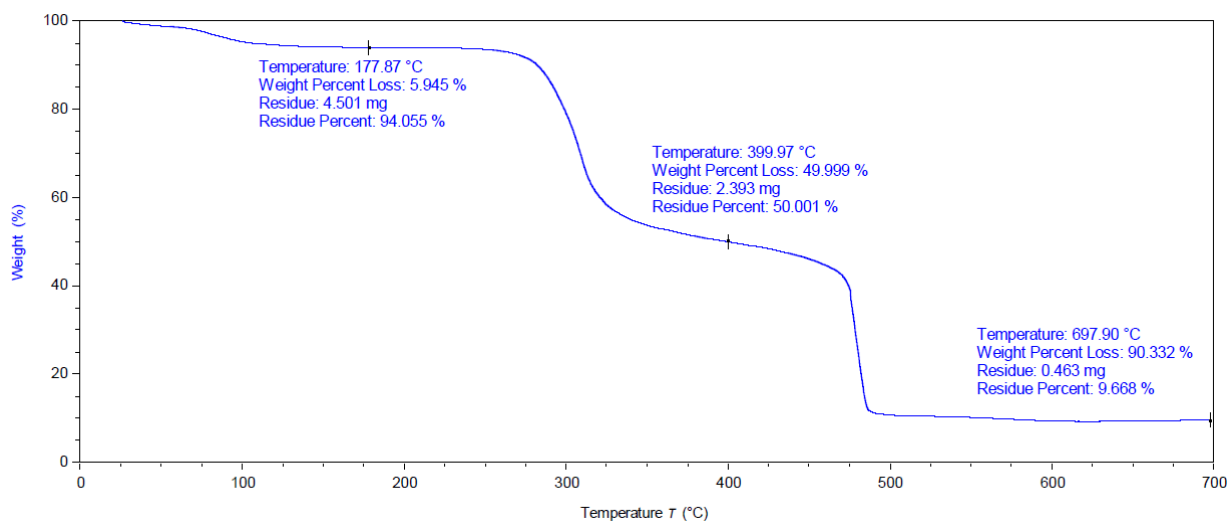


Figure S39. TGA thermogram of Fe-H2

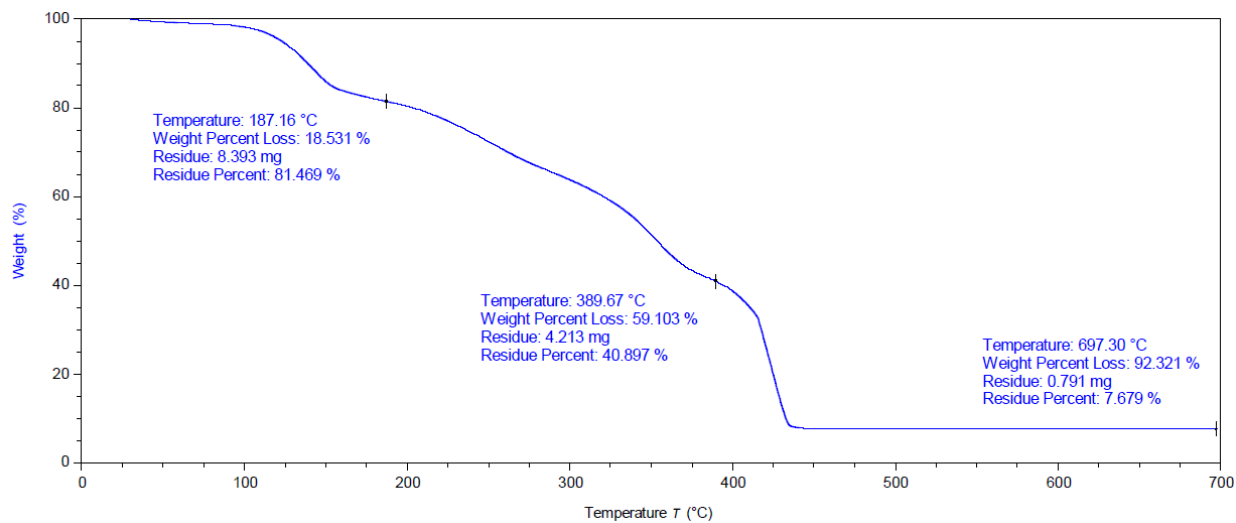


Figure S40. TGA thermogram of Fe-H3

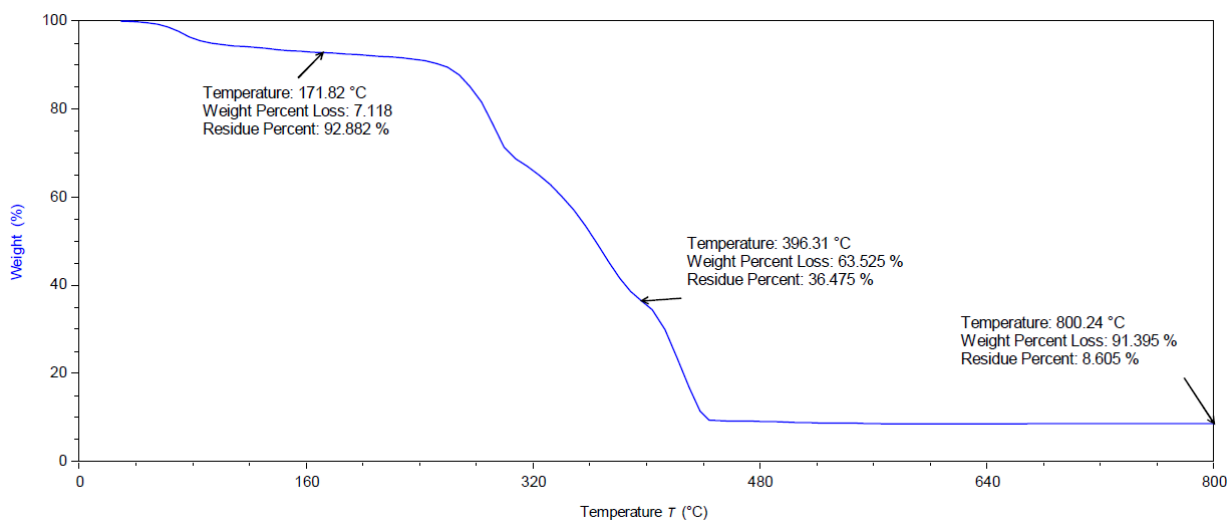


Figure S41. TGA thermogram of Fe-H4A

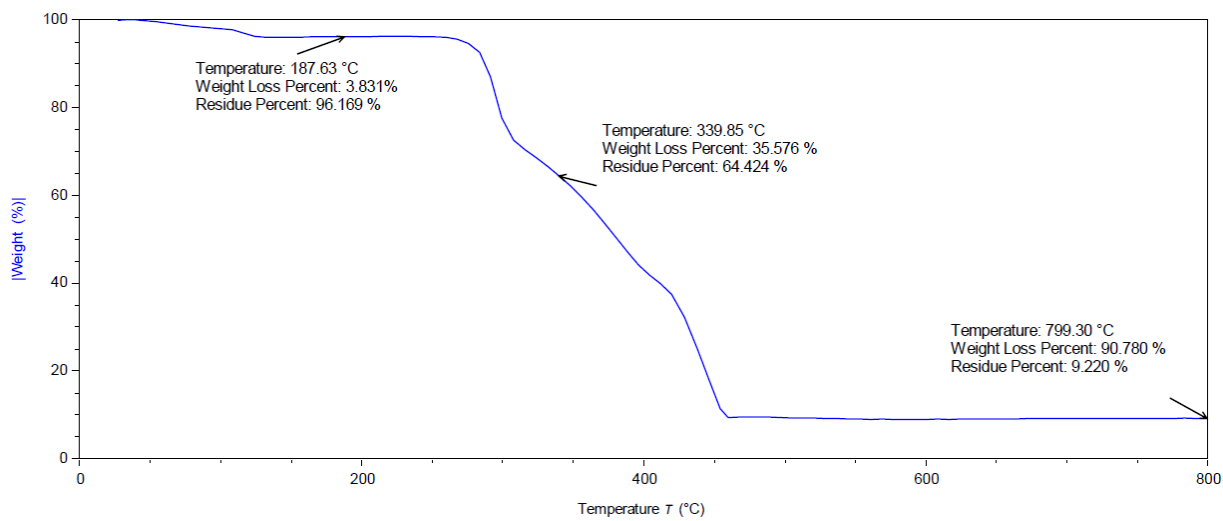


Figure S42. TGA thermogram of Fe-H4B

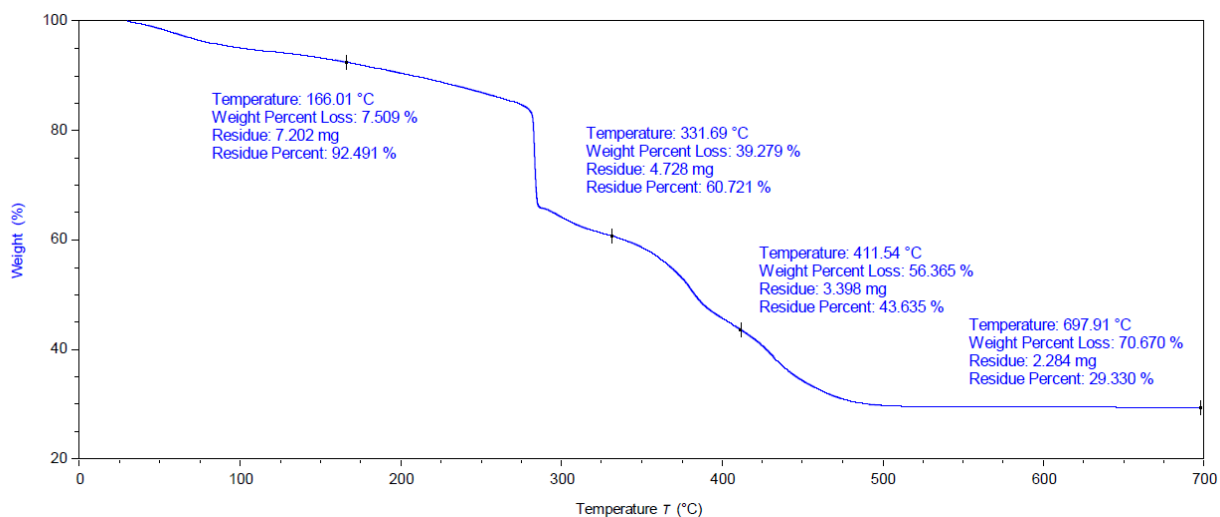


Figure S43. TGA thermogram of **Cu-H1**

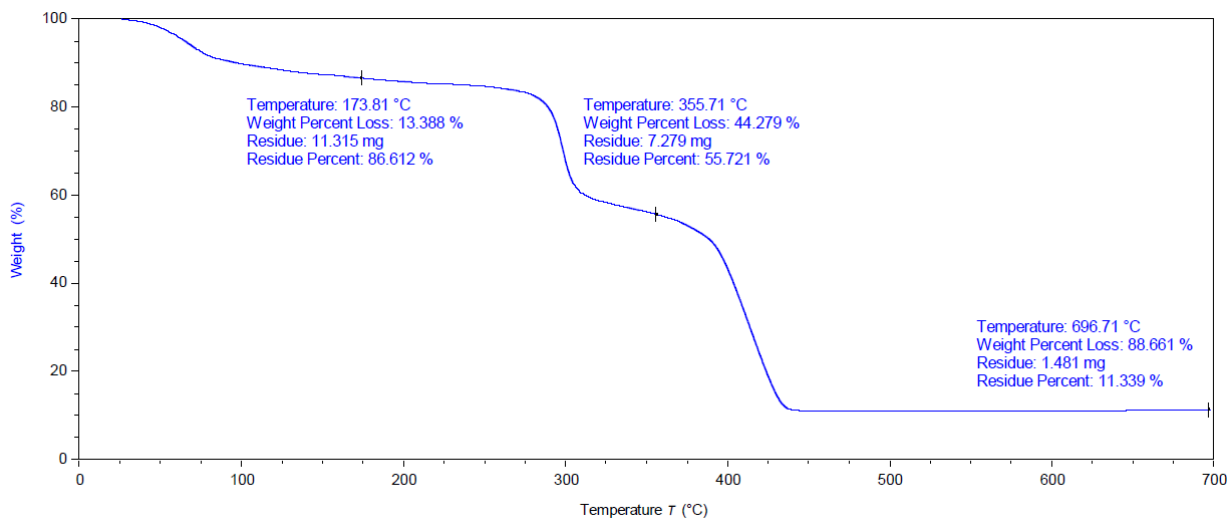


Figure S44. TGA thermogram of **Cu-H2**

9. References

- [1] G. M. Sheldrick, *Acta Cryst.* 2015, **A71**, 3-8.
- [2] G. M. Sheldrick, *Acta Cryst.* 2015, **C71**, 3-8.
- [3] A. L. Spek, *Acta Cryst.*, 2015, **C71**, 9-18